Evaluation of single-phase, discrete, mixture and combined model of discrete and mixture phases in predicting nanofluid heat transfer characteristics for laminar and turbulent flow regimes

EJ Onyiriuka[a], AI Obanor[b], M Mahdavi[c], DRE Ewim[d]

7 July 2018

[a,b]*Department of Mechanical Engineering, University of Benin, PMB 1154, Benin City, Edo State, Nigeria.*

[c,d]*Department of Mechanical and Aeronautical Engineering, University of Pretoria, Pretoria, Private Bag X20, Hatfield 0028, South Africa.*

[d] Corresponding author

E-mail address: daniel.ewim@up.ac.za (D.R.E. Ewim)

Phone: +27 (0) 604713246

Highlights

- Model evaluation in laminar and turbulent flow regimes for a nanofluid
- Model performance for a range of volume fraction.
- The mixture model and the combined model gave unrealistic results for both regimes.
- The discrete phase model was considerably accurate for both flow regimes.
- The single-phase model with constant properties gave good results for laminar flow.

Graphical abstract

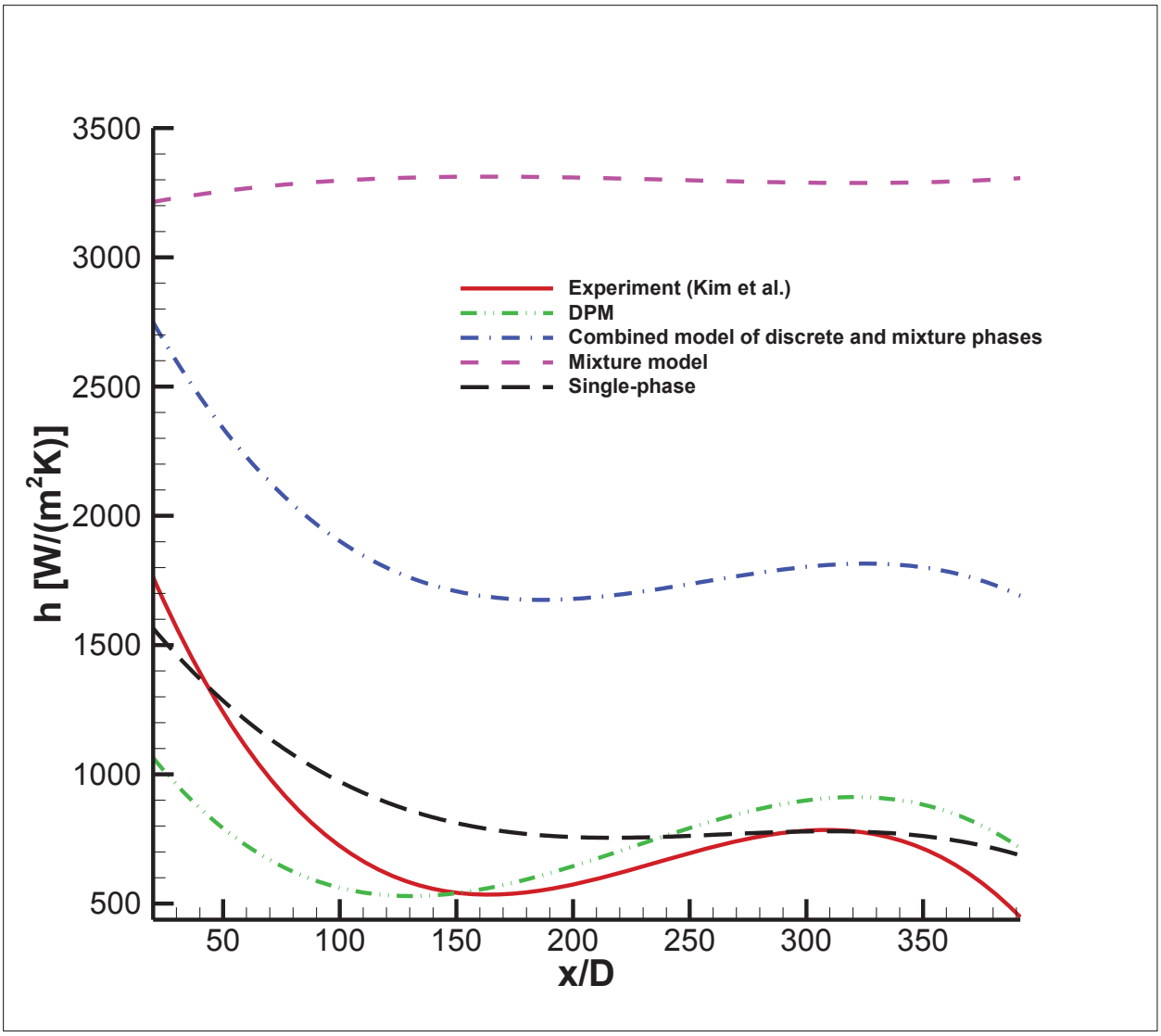

ABSTRACT

It is essential to investigate the appropriate model for simulating nanofluid flow for different flow regimes because, at present, most previous studies do not agree with each other. It was, therefore, the purpose of this study to present a Computational Fluids Dynamics (CFD) investigation of heat transfer coefficients of internal forced convective flow of nanofluids in a circular tube subject to constant wall heat flux boundary conditions. A complete three-dimensional (3D) cylindrical geometry was used. Laminar and turbulent flow regimes were considered. Three two-phase models (mixture model, discrete phase model (DPM) and the combined model of discrete and mixture phases) and the single-phase homogeneous model (SPM) were considered with both constant and variable properties. For the turbulent flow regime, it was found that the DPM with variable properties closely predicted the local heat transfer coefficients with an average deviation of 9%, and the SPM deviated from the DPM model by 2%. It was also found that the mixture and the combined discrete and the mixture phase model gave unrealistic results. For laminar flow, the DPM model with variable properties predicted the heat transfer coefficients with an average deviation of 9%.

Keywords

nanofluid, forced convection, discrete phase model, single-phase, two-phase

Nomenclature

$A_0, A_1, C_1, C_2, C_{1\epsilon}, C_{2\epsilon}$	RANS model constants
$\vec{a}$	Particle acceleration
Cp	Specific heat transfer, J/kg K
$cst.$	Constant properties
D	Tube diameter, m
DPM	Discrete phase model
d	Nanoparticle diameter, m
F	Body force, N
g	Gravitational acceleration, m/s^2
G_K	Generation of turbulent kinetic energy
Gz	Graetz number, $VD^2/\alpha L$
H	Total enthalpy, kJ/kg
h	Heat transfer coefficient, $\mathrm{W/m^2}$ K
k	Thermal conductivity, W/mK
L	Tube length, m
m	Mass, kg
Nu	Nusselt number, hD/k
P	Pressure, Pa
Pr	Prandtl number, $Cp\mu/k$
q	Wall heat flux, $\mathrm{W/m^2}$
r	Radial coordinate, m
r_0	Tube radius, m
RANS	Reynolds average Navier Stokes
Re	Reynolds number, $\rho VD/\mu$
Sm, Se	Source and sink terms
SPM	Single phase model
T	Fluid temperature, K
T^*	Dimensionless temperature, $(T - T_w)\ /(T_b - T_w)$

t	Time, s
v	Velocity vector, $\mathrm{m/s}$
v_{dr}	Drift velocity, $\mathrm{m/s}$
δV	Cell volume, $\mathrm{m^3}$
$var.$	Variable properties
x	Axial coordinate, (m)

Greek letters

ϵ	Dissipation rate of turbulent kinetic energy $(\frac{m^2}{s^3})$
K	Turbulent kinetic energy
κ	Kinematic viscosity
σ_t	Constant for turbulent Prandtl number
σ_K	Effective Prandtl number for turbulent kinetic
σ_ϵ	Effective Prandtl number for the rate of dissipation
τ_D	Time
α	Thermal diffusivity, $\mathrm{m^2/s}$
μ	Dynamic viscosity, Pa s
ρ	Density, $\mathrm{kg/m^3}$
ϕ	Particle volume fraction
τ	Wall shear stress, Pa
k_B	Boltzmann constant, 1.3807×10^{-23} J/K
μ_t	Turbulent molecular viscosity
ω	Angular velocity
υ	Kinematic viscosity, $\mathrm{m^2/s}$

Subscripts

av	average
b	bulk mean
bf	base fluid
i	inlet
m	mixture
n	total number of particles

nf	nanofluid
p	nanoparticle
w	wall
0	reference to inlet condition

1. Introduction

Nanofluids are a suspension of nano-meter sized solid particles either metallic or nonmetallic dispersed in a base heat transfer fluid which could be water, ethylene glycol or some other fluids. Some common nanoparticles include alumina, silica, copper oxide (CuO), titanium oxide (TiO_2) [1-11]. Most recently, nanoparticles have even been synthesized from biomaterials [12, 13]. The inclusion of these metallic oxides augment the thermal conductivity of the nanofluids significantly as the thermal conductivity of the particles is usually some orders higher in magnitude in comparison to the base fluid. In general, it can be concluded that nanofluids have shown great prospects and implications for a wide range of heat transfer and other applications [12, 14-19] such as electronic cooling, heat exchangers, air conditioning, automotive, nuclear system cooling, heating buildings, reducing pollution, storing energy [15, 17, 20-22].

Some recent works have been carried out on nanofluids by researchers using various innovative methods to study the complex heat and fluid dynamic interactions in the flow. Shirvan et al [23] numerically studied a heat exchanger filled with nanofluid. In their study, the response surface methodology and two-phase mixture model was used to carry out the sensitivity analysis of heat transfer and heat exchanger effectiveness in a double pipe heat exchanger filled with Al_2O_3 nanofluid. Ijaz et al. [24] presented a comprehensive study on the liquid and solid particles interaction propagating through a finite symmetric wavy channel. Bahiraei et al [25] carried out an assessment and optimization of hydrothermal characteristics for a non-Newtonian nanofluid (Cu nanoparticles in a base solution of 0.4 wt % carboxymethyl cellulose (CMC) in water) flow within miniaturized concentric-tube heat exchanger where he considered it from the designer's viewpoint in order to find the optimal cases with maximum heat transfer and minimum pressure drop. Bahiraei et al. [26] carried out a CFD simulation of the irreversibility caused by heat transfer and friction for a power-law nanofluid in a mini-channel having chaotic perturbations. The flows were laminar and turbulent regimes were not applicable. The convective heat transfer rate was reported to be limited due to poor flow mixing. Ellahi et al. [27] devoted a study to explore the credible potential use of kerosene-alumina nanofluid for thrust chamber regenerative cooling in semi-cryogenic rocket engine due to its enhanced thermal properties. Bhatti et al. [28] studied the peristaltic transport of two-phase (fluid-particle) flow. Rashidi et al [29] used the volume of fluid model to simulate the nanofluid flow and entropy generation in a single slope

solar still. They investigated the potential of Al_2O_3-water nanofluid to improve the productivity of a single solar slope still. Rahmat and Ellahi [30] state that the materials that advance the state-of-art of experimental, numerical and theoretical methodologies are still insufficient. Hence the need for more studies on nanofluid.

Over the years, there have been several experimental and numerical studies on heat transfer characteristics of the flow of nanofluids in tubes carried out by researchers [2, 3, 6, 8, 10, 17, 31-73]. A quick review of the most relevant works is presented below.

Kim et al. [31] experimentally studied the convective heat transfer characteristics of nanofluids in a straight circular tube under laminar flow conditions with constant wall heat flux. They used alumina nanofluid containing 3 vol% of suspended particles and found a 15% increase in the heat transfer coefficient at the early entrance region.

Wen and Ding [68] carried out an experimental investigation into convective heat transfer of nanofluid made of Υ-Al_2O_3 nanoparticle and de-ionized water flowing through a copper tube under laminar flow (Re < 2300) conditions and found that the enhancement was particularly significant in the entrance region.

Numerical investigation of forced convective heat transfer for water Al_2O_3 nanofluid inside a circular tube under constant wall heat flux has been investigated by several researchers [6, 32, 36, 43]. Furthermore, some researchers devised new models to simulate nanofluids based on their opinions on which phenomenon contributed more to the nanofluid's behavior [33, 36, 37, 56, 74, 75]. Several models have been used to simulate nanofluids. Some models used include the single-phase model and two-phase models: mixture model, discrete phase model, combined model of discrete and mixture phases but not all the models accurately predicted the heat transport properties of nanofluid with respect to the flow regimes. For example, Albojamal and Vafai [35] used a two dimensional (2D) fluid domain in his study and found that the mixture model only succeeded to accurately predict the heat transfer coefficient of the Al_2O_3/water nanofluid in a circular pipe under constant wall heat flux at a low volume fraction (ϕ) < 1% and for the developing region. The converse was true in other regions. He suggested the single-phase model for modeling nanofluids, since it gave results with good agreement with experimental data for the fully developed region with a maximum discrepancy of 5%. However, the single-phase

models require that the nanofluid under investigation has correlations that accurately represents its thermophysical properties before we can use the single-phase model. Additionally, the single-phase model therefore only solves but does not capture the physics of the particle-fluid interactions and does not give information of the secondary phase as a two-phase model will.

Mahdavi et al. [75] proposed a combined model of discrete and mixture phase for nanoparticles in turbulent convective flow in a horizontal tube. They implemented Brownian motion in the discrete phase model to predict the migration of the particles and the energy equation was modified for particles. The final results were then exported to the mixture equations of flow. They compared their results for friction coefficient and heat transfer coefficient with experimental results and found that their results deviated by less than 10% for most of the cases. However, the focus of their work was the details of changes in fluid flow and particles migration.

Bianco et al. [6] numerically investigated a developing laminar forced convective flow of water-Al_2O_3 nanofluid in a circular tube under constant wall heat flux. They assumed that the flow and thermal field are symmetrical with respect to the vertical plane passing through the tube main axis; hence they considered half of the tube. They used a single and two-phase model (discrete phase model) with either constant or temperature-dependent properties. They found that the heat transfer coefficient predicted by the single phase and discrete phase model had a maximum difference of 11% from each other. They also found that the heat transfer coefficients were higher in the case of temperature dependent models.

Mahdavi et al. [76] carried out a comparative study on simulation of convective Al_2O_3-water and ZrO_2-water nanofluid where they stated that lack of hybrid models for properties of nanofluids in different conditions was a problem hampering industrial applications. They investigated the single phase homogenous model, discrete phase model and the mixture model. Comparing appropriate turbulence models, they found the k-ε Realizable model was the best turbulence model for simulating nanofluid transport. They also stated that the mixture model was more consistent with experimental data for turbulent flow than the discrete phase model, they also noted that the discrete phase model could only be relied on for lower volume fractions less than 1.8%.

Albojamal and Vafai [35] carried out an evaluation of single phase, discrete and mixture models in calculating nanofluid transport. In his study, he used a two-dimensional axisymmetric assumption which was contrary to Mahdavi [33] who opined that it was important to use a three-dimensional (3D) model in nanofluid flow especially where gravity is present in the Lagrangian approach. They argued that two-dimensional axisymmetric only captures radial migration of nanoparticles inside the fluid whereas the difference between a three-dimensional and a two-dimensional axisymmetric simulation results show that nanoparticles migrated from the wall both radially and tangentially.

The review of previous works shows that there is still a gap in the open literature on the appropriate model for simulating nanofluid flow as results were obtained by researchers [1, 4, 6-8, 11, 32, 33, 35, 37, 77-79] who made important assumptions about the geometry. Albojamal and Vafai [35] used a two dimensional (2D) axisymmetric assumption which Mahdavi [33] argued was not sufficient to capture tangential migrations from the wall. While Bianco et al. [6] assumed that flow and thermal field were symmetrical and therefore considered half of the tube. The review also shows that there are some disagreements amongst researchers as to which model is good for simulating nanofluid flow under different flow regimes. Bianco et al. [6] compared the results of the ratio of local Nusselt number to local Nusselt number of the base fluid for $\phi = 1\%$, reported at x/D = 26 and 63 for Re = 1050 with experimental data of Wen and Ding [68] and found that the discrete phase model with temperature dependent properties had lower difference with a maximum gap being 3.5% at x/D = 63. In addition, Albojamal and Vafai [35] stated that the single phase model was more accurate in predicting heat transfer coefficient in laminar flow. He also stated that there were issues with regards to correlations for predicting thermal conductivity and viscosity accurately and the single phase model is only possible when these correlations are available and reliable. This dependence on correlations makes the single phase model difficult to use in cases where correlations are not available. In addition, the single phase model does not provide information about the secondary phase. Kristiawan et al. [7] carried out a numerical study of laminar convective heat transfer of TiO_2/water nanofluids of volume fractions 0.24, 0.6, 1.18 % using two-phase mixture model and found that the mixture model accurately predicted the heat transfer coefficients.

It was, therefore, the purpose of this study to investigate forced convective flow of nanofluid inside a complete three dimensional (3D) circular tube without assumptions about the geometry under constant wall heat flux boundary condition. ANSYS FLUENT software using finite volume method was used to solve the governing equations. Four models were studied and used for the simulation: single-phase and two-phase (which included Eulerian-Lagrangian and mixture models, and the novel combined model of discrete and mixture phases) to evaluate the accuracy in predicting the heat transfer coefficient of the nanofluid between the investigated models taking into account constant and temperature dependent thermo-physical properties for the two main flow regimes encountered and established in literature and in practice: the laminar and turbulent flow regimes. The results were compared with the experimental results of Kim et al. [31].

2. Thermophysical properties of the nanofluid for a single-phase mode

The thermophysical properties of solids are higher than conventional heat transfer fluids like water. Dispersion of the solids as small particles $\leq$ 100 nm in diameter in a heat transfer fluid can improve the inherently low thermo-physical properties of the fluid. The thermo-physical properties of the base fluid (water) and the alumina particles are given in Table 1. Researchers have proposed several correlations for calculating thermo-physical properties like thermal conductivity, density, viscosity, and heat capacity, but there are still problems regarding the proper correlations for predicting thermal conductivity and viscosity within an acceptable range Khanafer and Vafai [22].

2.1.Nanofluid density and specific heat

The following equations are used to estimate the density and specific heat capacity of the nanofluid [22, 80-82].

$$\rho_{nf} = (1-\phi)\rho_{bf} + \phi\rho_p \quad (1)$$

$$Cp_{nf} = (1-\phi)Cp_{bf} + \phi Cp_p \quad (2)$$

2.2. Nanofluid dynamics viscosity

2.2.1. Constant properties

Table 1. Physical properties of the base fluid and nanoparticles at T_i = 295K [35, 83]

Properties	Water	Al_2O_3
Cp (J/kgK)	4181	733
k (W/mK)	0.6	36
ρ $(kg/m\text{^}3)$	997.86	3880
$\mu(kg/ms)$	0.000955	-

Table 2. Heat transfer coefficient h [kW/m^{2}K], calculated for various Reynold numbers based on Williams et al. [97] experimental data

Re	T_{in} [K]	q [kW/m^2]	ϕ = 0.009 Williams et al. [97] h_{av}[kW/m^{2}K]	ϕ = 0.009 Present study h_{av}[kW/m^{2}K]	% Deviation
17417	295.950	94.391	9.600	8.000	16.7
29178	311.950	95.204	16.300	12.500	23.3
30140	294.550	93.568	14.200	12.800	9.9
31230	301.050	170.146	16.500	13.200	20.0

For constant properties, the effective viscosity depends only on the volume fraction ϕ, Maiga et al. [34] based on experimental data, carried out a least-square curve fitting, which led to the correlation:

$$\frac{\mu_{nf}}{\mu_{bf}} = 1 + 7.3\phi + 123\phi \tag{3}$$

It is worthy to note that when we refer to constant properties, we are referring to a property with no variation with respect to temperature.

2.2.2. Temperature-dependent properties

Corcione [46] developed temperature-dependent properties for dynamic viscosity using best-fit and recommended the following correlation with 1.84% standard deviation of error.

$$\frac{\mu_{nf}}{\mu_{bf}} = 1 - 34.87\left(\frac{d_p}{d_f}\right)^{-0.3}\phi^{1.03} \tag{4}$$

$$d_f = 0.1\left(\frac{6M}{N\pi\rho_f}\right)^{1/3} \tag{5}$$

It is also worthy to note that when we refer to temperature dependent properties, we mean that the properties are changing with temperature.

2.3. Nanofluid thermal conductivity

2.3.1. Constant properties

Maiga et al. [34] carried out the same procedure used for dynamic viscosity for thermal conductivity. The correlation is.

$$\frac{k_{nf}}{k_{bf}} = 1 + 2.72\phi + 4.97\phi^2 \tag{6}$$

2.3.2. Temperature-dependent properties

Corcione [46] recommended the following correlation which he obtained by regression analysis with 1.86% standard deviation error.

$$\frac{k_{nf}}{k_{bf}} = 1 + 4.4{Re_p}^{0.4}{Pr_f}^{0.66}\left(\frac{T_{nf}}{T_{fr}}\right)^{10}\left(\frac{k_p}{k_f}\right)^{0.03}X^{0.66} \tag{7}$$

$$Re_p = \frac{\rho_f u_B d_p}{\mu_f} = \frac{2\rho_f \kappa_b T_{nf}}{\pi \mu_f{}^2 d_p} \quad (8)$$

Proper polynomial thermo-physical properties of water as the base fluid was chosen from a simple curve fitting which is available in heat transfer textbooks and the technical literature McNab and Meisen [84].

$$\mu_{bf} = 0.414092804247831 - 4.792184560427 \times 10^{-3} \times T + 2.0927097596 \times 10^{-5} \times T^2 - 4.0781184 \times 10^{-8} \times T^3 + 2.9885 \times 10^{-11} \times T^4 \quad (9)$$

$$\rho_{bf} = 765.33 + 1.8142 \times T - 0.0035 \times T^2 \quad (10)$$

$$Cp_{bf} = 10444.58656104 - 54.08920728 \times T + 0.15359377 \times T^2 - 0.00014301 \times T^3 \quad (11)$$

$$k_{bf} = -0.46662403 + 0.00575419 \times T - 7.18 \times 10^{-6} \times T^2 \quad (12)$$

3. Boundary conditions and geometrical configuration

A complete three dimensional (3D) geometry was considered as shown in Fig. 1(a) with a non-uniform mesh with fine mesh at the wall as shown in Fig.1(b) to capture the near wall behavior of the fluid while at the axis of the tube is relatively coarse since flow properties are expected to change more gradually. To ensure fully developed flow in the tube outlet section, the tube was chosen to be long enough. The tube is subjected to a constant wall heat flux condition with a uniform temperature profile and axial velocity at the inlet section. The nanofluid is made of water with Al_2O_3 particles of an average of 20 nm in size.

3.1.Grid generation method and independence study

The element mid-side nodes were dropped and the curvature sizing function was used to examine the curvature on the edges and faces and computed element sizes on these entities such that the size will not violate the maximum size or curvature angle. The relevance center was chosen to be fine so that the element size was reasonably small. Inflation layers were used to capture near wall physics.

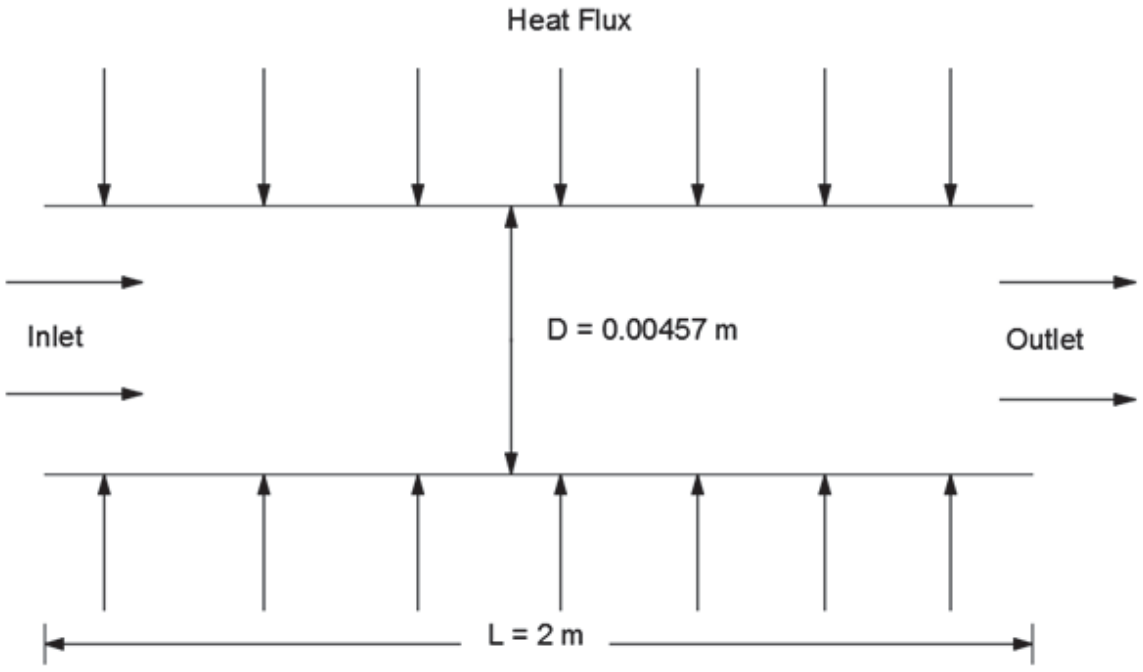

Figure 1(a) Geometrical configuration for the present study.

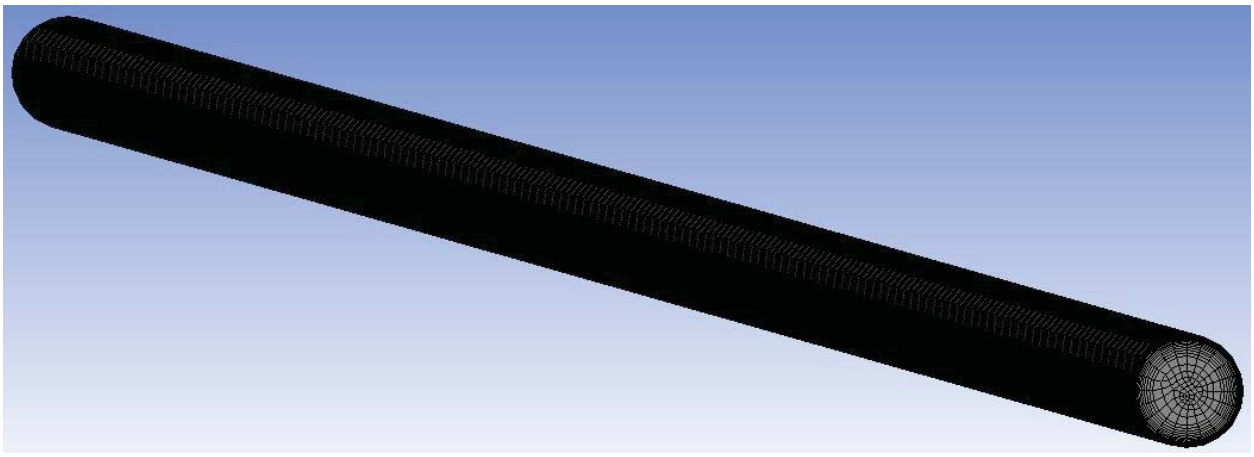

Figure 1(b) Mesh for the present study.

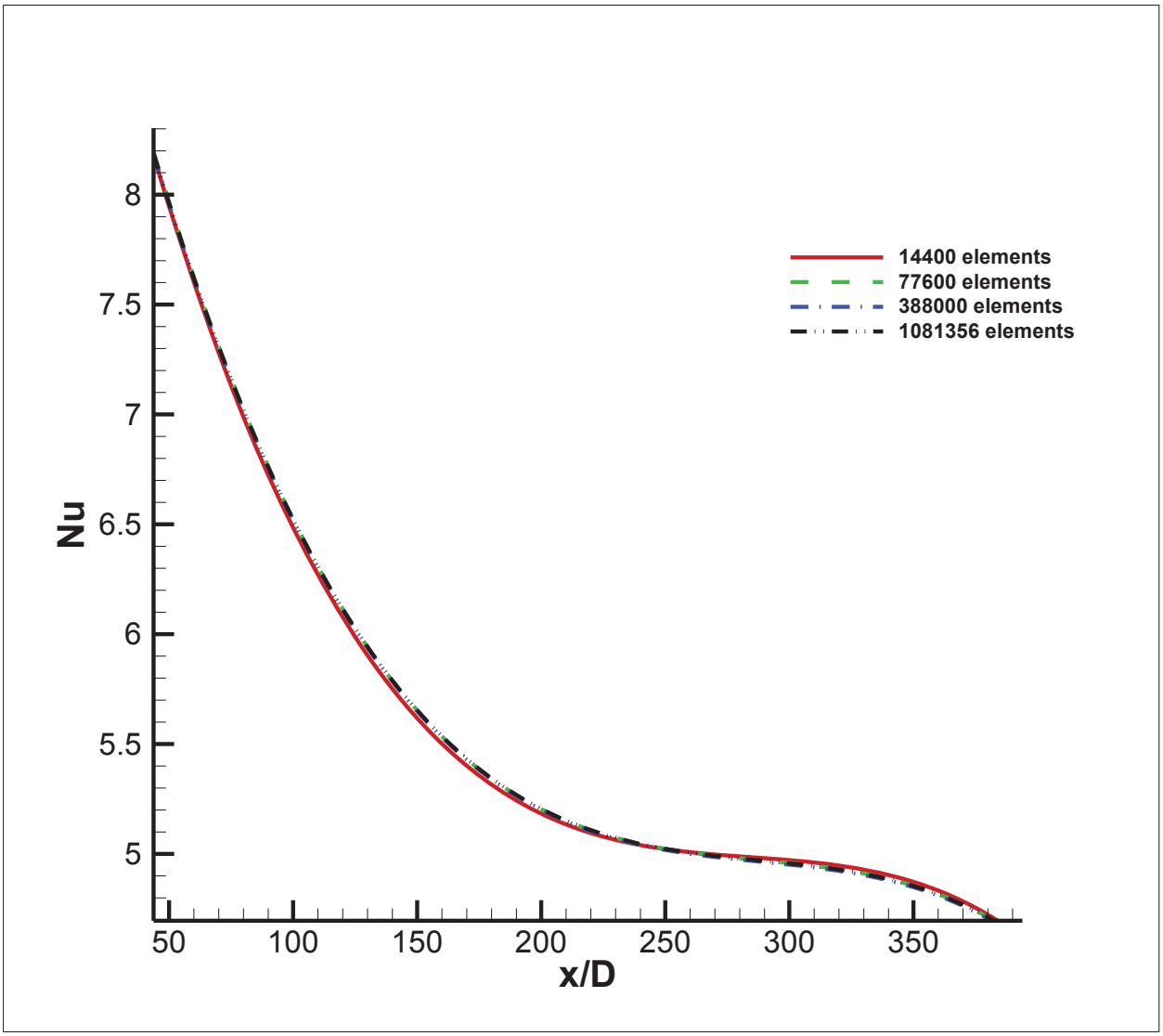

Figure 2 Grid independence result.

For a grid independence test four grid densities 14400, 77600, 388000, 1081356, were used as shown in Fig.2. Graphs of local Nusselt number were observed for Re = 1620 and q = 2089.56 W/m^2. There was less than 0.2% difference between the 1081356 and 388000 elements. Hence the latter was chosen for the simulation.

4. Solution scheme

The fluid and the solid phase was considered to be coupled using two-way coupling during the simulation. Meaning that the fluid can alter the particle motion via drag, and the particles could interchange energy and momentum with the continuous fluid. The commercial code ANSYS FLUENT was used, which is based on the finite volume method and the SIMPLE algorithm couples pressure and the velocity fields. PRESTO scheme for pressure, QUICK for volume fraction and SECOND ORDER UPWIND for other parameters were considered to discretize the governing equations.

In the discrete phase model, 600 and 900 flow iterations were completed per DPM iteration for laminar and turbulent flow. When particle trajectories are resolved, and interphase exchange of the momentum, heat, and mass in the control volume are updated, these interphase exchange terms disturbs the continuous phase when the continuous phase iterations are calculated. Convergence was reached when the continuous phase flow no longer varied with further calculations, and when this happened, the discrete phase trajectories was no longer disturbed since changes in the discrete phase trajectories would lead to changes in the continuous phase flow field [85]. In this study, the convergence criterion was met when residuals fall below 10^{-6} and drag coefficient was also monitored to not change with iterations.

5. Mathematical modeling

5.1. Homogenous single-phase approach

Under this approach, the nanofluid was considered as a homogenous fluid flow with improved thermophysical properties of which the thermal conductivity and viscosity depend on correlations drawn from experimental data. Also, this model takes the liquid and particle phases as in thermal equilibrium and that they move with the same velocity [86].

The dimensional governing equations for steady state single-phase model are as follows [6, 40, 80, 81]:

Continuity

$$\nabla.\left(\rho_{nf}\vec{v}\right) = 0 \tag{13}$$

Momentum

$$\nabla.\left(\rho_{nf}\vec{v}\vec{v}\right) = -\nabla P + \nabla.\left(\mu_{nf}\nabla\vec{v}\right) \tag{14}$$

And Energy

$$\nabla.\left(\rho_{nf}\vec{v}\ Cp\ T\right) = \nabla.\left(k_{nf}\nabla\ T\right) \tag{15}$$

5.2. Lagrangian-Eulerian approach (DPM)

In the Lagrangian-Eulerian model (or discrete-phase model) it is considered that the fluid is a single fluid with two phases which are strongly coupled with the continuous phase being taken as a continuum and the dispersed phase (particles) can exchange mass, momentum, energy with the continuous fluid-the base fluid. A major assumption made in this approach is that the dispersed phase is adequately diluted in such a way that particle-particle interactions are virtually negligible [85].

The mathematical formulation of the Lagrangian-Eulerian two-phase model is given below [17, 80, 87]:

Continuity,

$$\nabla.\left(\rho_{nf}\vec{v}\right) = 0 \tag{16}$$

Momentum,

$$\nabla.\left(\rho_{nf}\vec{v}\vec{v}\right) = -\nabla P + \nabla.\left(\mu_{nf}\nabla\vec{v}\right) + S_m \tag{17}$$

And Energy,

$$\nabla.\left(\rho_{nf}\vec{v}\ Cp\ T\right) = \nabla.\left(k_{nf}\nabla\ T\right) + S_e \tag{18}$$

Source/Sink terms $s_m$and s_e represent the combined effects of the momentum and energy exchange with the base fluid as the particles move through the Eulerian phase of the base fluid with the volume of δV. It is worthy to note that in the case of single-phase the source/sink terms are both equal to zero.

The exchange of momentum between the particles and the base fluid is calculated as Mirzaei et al. [60]

$$S_m = \frac{1}{\delta V}\sum_{p=1}^{n}\vec{F}_p \tag{19}$$

In the Lagrangian reference frame, a force balance equates the particle inertia with the forces acting on the particle, and the trajectories of particles are calculated by integration.

$$m_p \frac{d\bar{V}_p}{dt} = F_D + F_g + F_L + F_B + F_T + F_p + F_v \tag{20}$$

where the left-hand side represents the particle inertia in which $\bar{V}_p$ is the particle velocity, m_p is the particle mass and the right hand side represents the forces acting on the particle which are the drag F_D, gravity F_g, Saffman's lift F_L, Brownian F_B, thermophoresis F_T, pressure gradient F_p and virtual mass force F_v respectively.

Correlations are used for each force term as follows

Drag force F_D is evaluated using Stokes' relationship for submicron particles, but only valid for $Re_d \leq 0.1$ where

$$Re_d = \frac{\rho d_p |\bar{v}_p - \bar{v}_c|}{\mu} \tag{21}$$

and,

$$F_D = \frac{18\mu}{d_p^2 \rho_p C_c}(\vec{v} - \vec{v}_p)m_p \tag{22}$$

where the factor C_c is the Cunningham

correction: $C_c = 1 + \frac{2\lambda}{d}(1.257 + 0.4e^{-\left(\frac{1.}{2\lambda}\frac{1d}{}\right)})$ (23)

where $\lambda = 0.17\,nm$ is the mean free path of the base fluid and $\vec{v}_c$ is the continuous phase velocity. Cunningham correction is necessary to apply the stokes' relationship to submicrometer particles [88, 89].

Gravity force F_g is defined as:

$$F_g = \frac{g(\rho_p - \rho)}{\rho} \tag{24}$$

Saffman's lift force F_L is found by Khanafer et al. [20]

$$F_L = \frac{2Kv^{1/2}\rho\, d_{ij}}{\rho_p d_p (d_{lk} d_{lk})^{1/4}} \left(\vec{v} - \vec{v}_p\right) \tag{25}$$

where K is the constant coefficient of Saffman's lift force and is equal to 2.594 and the rate deformation tensor $d_{ij} = \frac{1}{2}(u_{i,j} + u_{j,i})$.

It should be noted that this form of lift force is only recommended for submicron particles and is intended for small particle Reynolds number [90].

Brownian force F_B is determined by [85]

$$F_B = \zeta_i \sqrt{\frac{\pi\, S_0}{\Delta t}} \tag{26}$$

where ζ_i are zero-mean, unit-variance-independent Gaussian random numbers and $S_0 = \frac{216\, u\, k_B T}{\pi^2 \rho\, {d_p}^5 \left(\frac{\rho_p}{\rho}\right) C_c}$

where k_B is the Boltzmann constant

Thermophoresis force F_T is determined by the correlation suggested by Talbot et al. [91].

$$F_T = \frac{6\pi d_p \mu^2 C_s \left(\frac{k}{k_p} + C_t K_n\right)}{\rho(1+3C_m K_n)\left(1+2\left(\frac{k}{k_p}\right)+2C_t K_n\right)} \frac{1}{m_p T} \nabla T \tag{27}$$

where

K_n is Kundsen number and is $2\lambda/d_p$, C_m is the momentum exchange coefficient and is 1.146, C_t is the temperature jump coefficient $= 2.18$, C_s is the thermal slip coefficient $= 1.147$

Pressure gradient force F_p is obtained by:

$$F_p = \left(\frac{\rho}{\rho_p}\right) V_p . \nabla V \tag{28}$$

where V is the axial velocity.

Virtual mass force F_v, the force required to accelerate the fluid surrounding the particle as it moves and it is given as:

$$F_v = C_{vm} \frac{\rho}{\rho_p} (\vec{v}_p \nabla \vec{\mathrm{v}} - \frac{d\vec{v}_p}{dt}) \tag{29}$$

where C_{vm} is the virtual mass-factor which has a default value of 0.5.

The energy balance of a particle can be stated as:

$$m_p Cp \frac{dT_p}{dt} = hA_p(T - T_p) \tag{30}$$

where h (heat transfer coefficient) is calculated from Ranz and Marshall's correlation[92]

$$Nu = \frac{h.d}{k} = 2 + 0.6Re^{1/2}Pr^{1/3} \tag{31}$$

We can obtain the energy exchange when we solve the energy balance equation:

$$S_e = \frac{1}{\delta V} \sum_{p=1}^{n} m_p Cp \frac{dT_p}{dt} \tag{32}$$

5.3. Mixture model

This model uses a single fluid two-phase approach; it assumes that local equilibrium between the phases is reached over a short spatial length scale and that there is a strong coupling between the phases. The mixture model is a simplified multiphase model. It solves the continuity, momentum, and energy equations. It also solves the volume fraction equation for the particulate phase, and then it uses an algebraic expression to calculate the relative velocity between the base fluid and the particle.

The dimensional equations of the mixture model governing equations are stated below [5, 32, 87]:

Continuity,

$$\nabla.(\rho_m \vec{v}_m) = 0 \tag{33}$$

Momentum,

$$\nabla.(\rho_m \vec{v}_m \vec{v}_m) = -\nabla p + \nabla.(\mu_m \nabla \vec{v}_m) + \nabla.\left(\sum_{k=1}^{n} X_k \rho_k \vec{v}_{dr,k} \vec{v}_{dr,k}\right) \tag{34}$$

Energy,

$$\nabla.[\sum_{k=1}^{n} \phi_k \vec{v}_k (\rho_k H_k + p)] = \nabla.(k \nabla T) \tag{35}$$

And volume fraction

$$\nabla.\left(\phi_p \rho_p \vec{v}_m\right) = -\nabla.(\phi_p \rho_p \vec{v}_{dr,p}) \tag{36}$$

$$\vec{v} = \sum_{k=1}^{n} \frac{\phi_k \rho_k \vec{v}_k}{\rho} \tag{37}$$

$$\rho = \sum_{k=1}^{n} \phi_k \rho_k \tag{38}$$

$$\mu = \sum_{k=1}^{n} \phi_k \mu_k \tag{39}$$

$$k = \sum_{k=1}^{n} \phi_k k_k \tag{40}$$

H_k is the sensible enthalpy for phases.

The drift velocity ($\vec{v}_{dr,k}$) for the secondary phase is

$$\vec{v}_{dr,k} = \vec{v}_k - \vec{v}_m \tag{41}$$

The relative or slip velocity is defined as the velocity of the second phase (p) relative to the velocity of the primary phase (f):

$$\vec{v}_{pf} = \vec{v}_p - \vec{v}_f \tag{42}$$

The drift velocity related to the relative velocity becomes

$$\vec{v}_{dr,p} = \vec{v_{pf}} - \sum_{k=1}^{n} \frac{\vec{v}_{fk}\phi_k\rho_k}{\rho_m} \quad (43)$$

and Manninen et al. [52] and Naumann and Schiller[93] proposed the following respective equations for relative velocity $\vec{v_{pf}}$ and the drag function f_{drag}.

$$\vec{v}_{pf} = \frac{\rho_p {d_p}^2}{18\mu_m f_{drag}} \frac{\rho_p - \rho_m}{\rho_p} \vec{a} \quad (44)$$

$$f_{drag} = \begin{cases} 1 + 0.15{Re_p}^{0.687} Re_p \leq 1000 \\ 0.0183 Re_p \; Re_p \geq 1000 \end{cases} \quad (45)$$

Here the acceleration is determined by

$$\vec{a} = \vec{g} - (\vec{v}_m . \nabla)\vec{v_m} \quad (46)$$

And d_p is the diameter of the nanoparticles of the secondary phases and $\vec{a}$ is the secondary phase particles acceleration.

The solids shear viscosity is given by the sum of collisional and kinetic parts and the optional frictional part.

The collisional part is a viscosity contribution due to collisions between particles taken from the kinetic theory of granular flow of Syamlal et al. [94].

$$\mu_{p,col} = \frac{4}{5}\phi_p\rho_p d_p g0,pp(1 + e_{pp})\left(\frac{\Theta_p}{\pi}\right)^{1/2}\phi_p \quad (47)$$

while for the kinetic viscosity part the Syamlal et al. [94] model is used to calculate it. The expression is given as:

$$\mu_{p,kin} = \frac{\phi_p d_p \rho_p \sqrt{\Theta_p \pi}}{6(3 - e_{pp})}\left[1 + \frac{2}{5}(1 + e_{pp})(3e_{pp} - 1)\,\phi_p g0,pp\right] \quad (48)$$

and the bulk viscosity is the granular particle's resistance to compression or expansion. The model is developed from the kinetic theory of granular flow based on Lun et al. [95].

$$\lambda_p = \frac{4}{3}\phi_p\rho_p d_p g0,pp(1 + e_{pp})\left(\frac{\Theta_p}{\pi}\right)^{1/2} \quad (49)$$

where, in Eqs (47-49) $g0, pp$ is the radial distribution function and Θ_p is the granular temperature and e_{pp} is the restitution coefficient and λ_p is the bulk viscosity.

5.4. A combined model of discrete and mixture phases

The numerical procedure for this model is as given by Mahdavi et al. [75]; they first solved the flow and energy equations for the base fluid in the turbulent regime to convergence then solved discrete phase for one iteration with Brownian force and particle heat transfer equation with turbulent particle diffusivity calculated and stored. Then the particles concentration is stored and the gradient of temperature is calculated. All fluid properties are changed and the source terms of energy equation implemented, and simulation goes to reach a final acceptable solution.

5.5. Turbulence modeling

The realizable $\kappa - \epsilon$ turbulent model was proposed by Shih et al. [54]. The equations for the turbulent kinetic (κ) and dissipation of turbulent kinetic energy (ϵ) used in the Realizable $\kappa - \epsilon$ turbulent model are given as

$$div(\rho\kappa\vec{v}) = div\left\{\left(\mu + \frac{\mu_t}{\sigma_k}\right) grad\ \kappa\right\} + G_k - \rho\epsilon \tag{50}$$

$$div(\rho\epsilon\vec{v}) = div\left\{\left(\mu + \frac{\mu_t}{\sigma_k}\right) grad\ \epsilon\right\} + \rho C_1 S_\epsilon - \frac{\rho\epsilon^2 C_2}{\kappa+\sqrt{\nu\epsilon}} \tag{51}$$

Here

$C_1 = max\left[0.43, \frac{\eta}{\eta+5}\right]$, $G_k = \mu_t S^2$, $\eta = S\frac{\kappa}{\epsilon}$ and $S = \sqrt{2S_{ij}S_{ij}}$

In these equations G_k represents the generation of turbulent kinetic energy due to the mean velocity gradients. Here, S is the modulus of the mean rate-of-strain tensor, σ_κ and σ_ϵ are the effective Prandtl numbers for the turbulent kinetic energy and the rate of dissipation respectively.

Hence, μ_t is modeled as

$$\mu_t = \frac{\rho\kappa^2}{\epsilon}\left(\frac{A_0}{A_s + A\frac{\kappa U^*}{\epsilon}}\right)^{-1} \tag{52}$$

Here, A_0 and A_s are the model constants given as

$A_0 = 4.04$ and $A_s = \sqrt{6}\cos\phi$ respectively with

$\phi = \frac{1}{3}\cos^{-1}\sqrt{6}W$, $U^* = \sqrt{S_{ij}S_{ij} + \tilde{\Omega}_{ij}\tilde{\Omega}_{ij}}$, $\tilde{\Omega}_{ij} = \bar{\Omega}_{ij} - 3\epsilon_{ijk}\omega_k$ and

$$W = \frac{S_{ij}S_{jk}S_{ki}}{\tilde{S}^3} \tag{53}$$

Here, $\tilde{\Omega}_{ij}$ is the mean rate of rotation tensor with the angular velocity ω_k. in Eqs. 50 and 51, the model constants are $C_1 = 1.44$, $C_2 = 1.9$, $\sigma_\kappa = 1.0$ and $\sigma_\epsilon = 1.2$

6. Results and discussion

The results were obtained first for pure water flowing inside a circular tube to evaluate the accuracy, grid independence, and the model. The Nusselt number obtained for *Re* = 1460 was validated with a correlation by Churchill and Ozoe [96] with an average error of less than 3% as shown in Fig. 3 for thermally and hydraulically developing flow with a uniform heat flux of 2089.56 W/m^2. The correlation by Churchill and Ozoe [96] is as follows:

$$\frac{Nu_D}{4.364\left[1+\left(\frac{Gz}{29.6}\right)^2\right]^{1/6}} = \left[1 + \left(\frac{\frac{Gz}{19.04}}{\left[1+\left(\frac{Pr}{0.0207}\right)^{2/3}\right]^{1/2}\left[1+\left(\frac{Gz}{29.6}\right)^2\right]^{1/3}}\right)^{3/2}\right]^{1/3} \tag{54}$$

And it agrees within 5% for *Pr* = 0.7 and *Pr* = 10 of other investigators' numerical data

The Nusselt number obtained for *Re* = 4600 in this current study is in a good agreement with Gnielinski's equation [55] as shown in Fig.4.

$$Nu(x) = \frac{\frac{f}{8}(Re-1000)Pr}{1+12.7\sqrt{\frac{f}{8}}(Pr^{\frac{2}{3}}-1)}\left[1+\left(\frac{d}{L}\right)^{2/3}\right] \tag{55}$$

$$f = \frac{1}{(1.8\log_{10}Re - 1.64)^2} \tag{56}$$

Next, the results of the nanofluid were validated for laminar flow using experimental data of Wen and Ding [68] for *Re* = 1050 and ϕ = 0.6% in Fig. 5. The figure showed good agreement of the present study with experimental results with a particularly high heat transfer coefficient at the entrance region as reported in their experimental results. Additionally, it should be noted that the

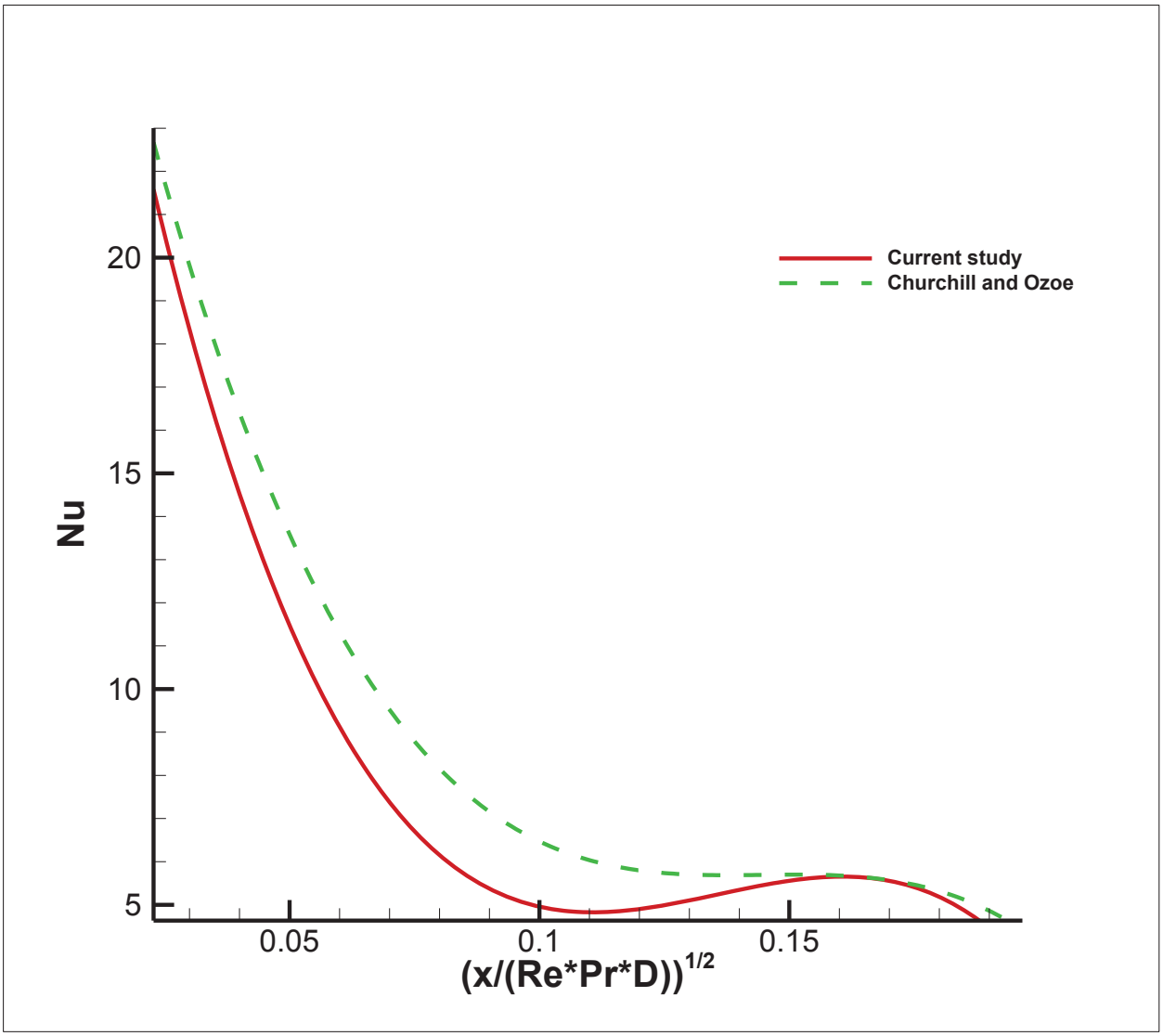

Figure 3. Model validation with Churchill and Ozoe's correlation [96].

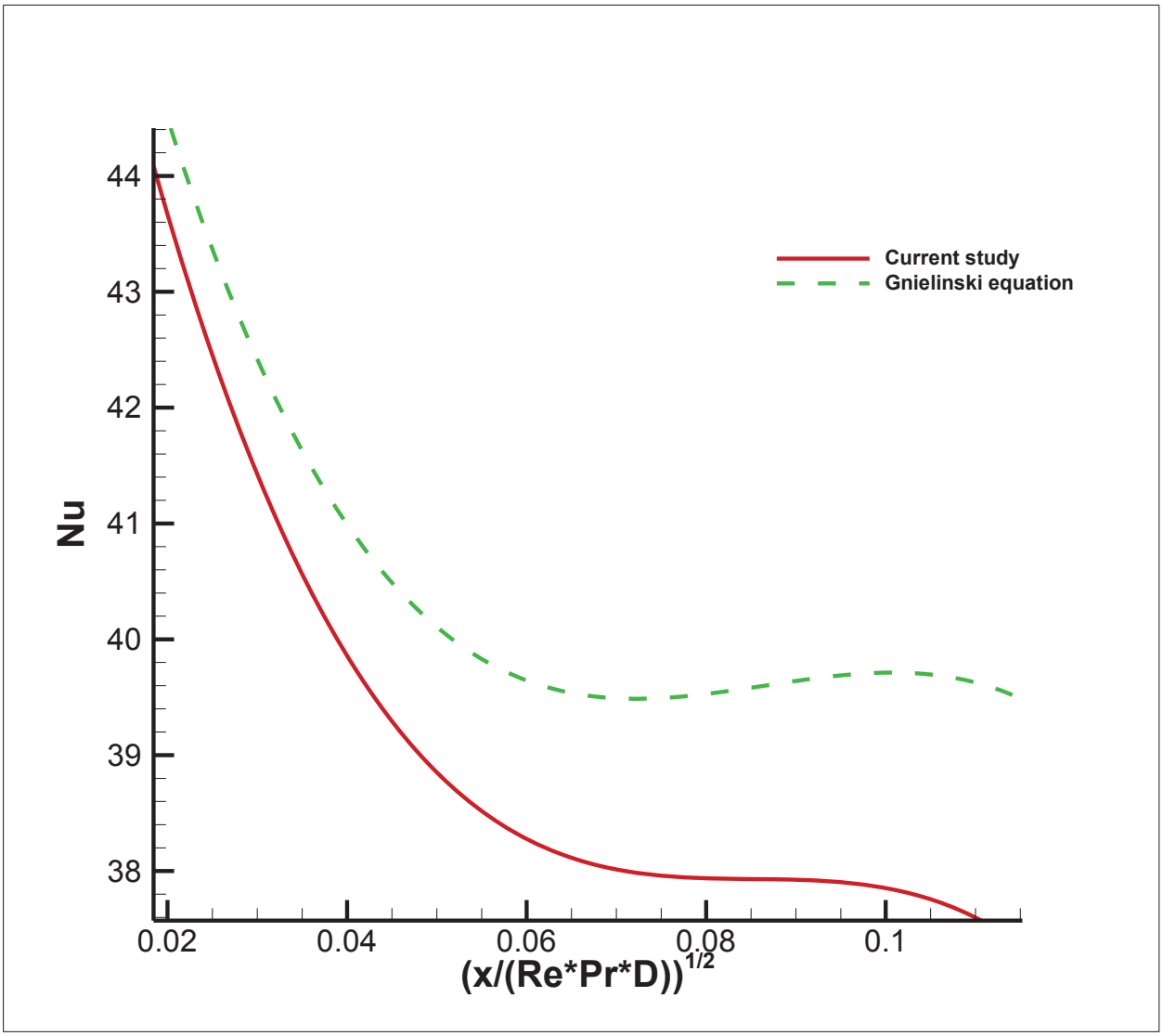

Figure 4. Model validation with Gnielinski equation [55].

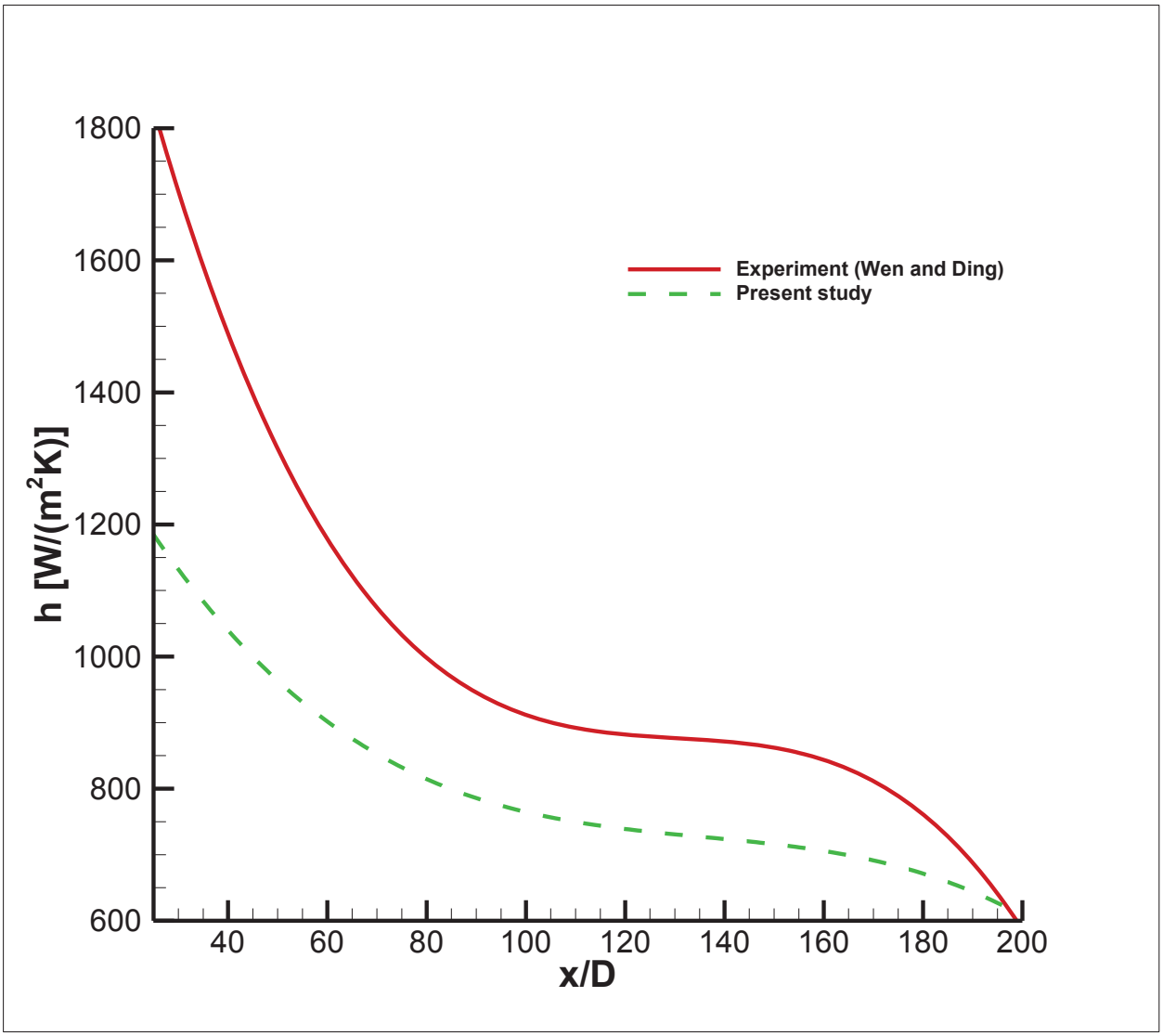

Figure 5. Nanofluid validation for laminar flow using experimental data of Wen and Ding [68] for Re = 1050 and = 0.6%.

highest deviation which was 35% from their experimental results was observed at the entrance region and the deviation reduces along the pipe's length. This deviation could be attributed to the limitation of modeling multiphase flows as their numerical methods have not yet been fully validated.

Results of the nanofluid were further validated for turbulent flow using experimental data of Williams et al. [97] as shown in Table 2. It can deduced from the table that a satisfactory agreement was found.

Four different models were used in the numerical simulation: single-phase homogenous, two-phase (Lagrangian-Eulerian, mixture phase and combined model of discrete and mixture phases) each with constant properties and temperature dependent properties to ascertain which model is best for nanofluid simulation under laminar and turbulent flow regimes. *Re* = 1460, *Re* = 6020 by comparison of all models with experimental data of Kim et al. [31] with particle loading of 3% and wall heat flux boundary conditions; q = 2089.56W/m^2.

Fig. 6 shows the profiles of dimensionless radial velocity along the tubes radius at different axial locations up to x/L = 0.4 for *Re* = 1460, q =2089.56 W/m^2 and ϕ = 3% using the single phase model. The hydrodynamic entry length is given by $L_{h,laminar} = 0.05 Re_D D$ [98, 99] which evaluates to x = 0.3 m from the inlet section. It can be observed that the nanofluid is fully developed at an entrance length of 0.4 m. It should be noted that the mean velocity is different for different nanoparticle volume fraction to maintain a constant Reynolds number. This may be attributed to the fact that the Reynolds number depends on the density and viscosity of the fluid which varies directly with the nanoparticle volume fraction. In addition, the nanofluid's viscosity increases faster than the density as the volume fraction of nanoparticles is increased.

Fig. 7 shows the profiles of dimensionless radial velocity along the tubes radius at different axial locations up to x/L = 0.4 for *Re* = 6020, q = 2089.56 W/m^2 and ϕ = 3% using the single phase model. The hydrodynamic entry length is given by $L_{h,turbulent} = 1.359 D\ Re_D^{\frac{1}{4}}$ [100, 101] which evaluates to 0.05 m from the inlet section. It can be seen that the nanofluid under turbulent flow is fully developed at 0.08 m. It should be noted that the entry length is much shorter in turbulent

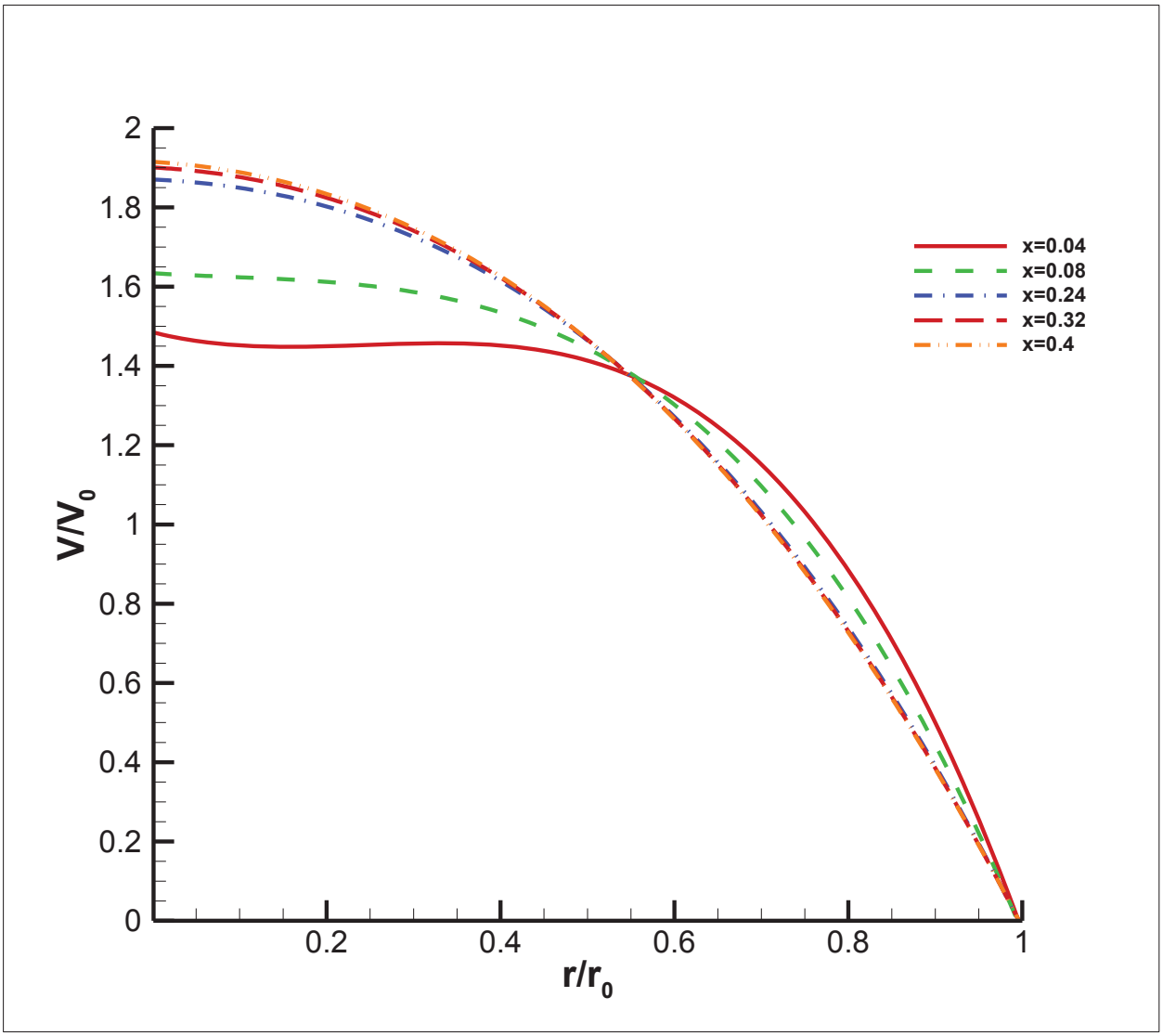

Figure 6. Radial velocity profiles for q = 2089.56 W/m^2, Re = 1460 and = 3%.

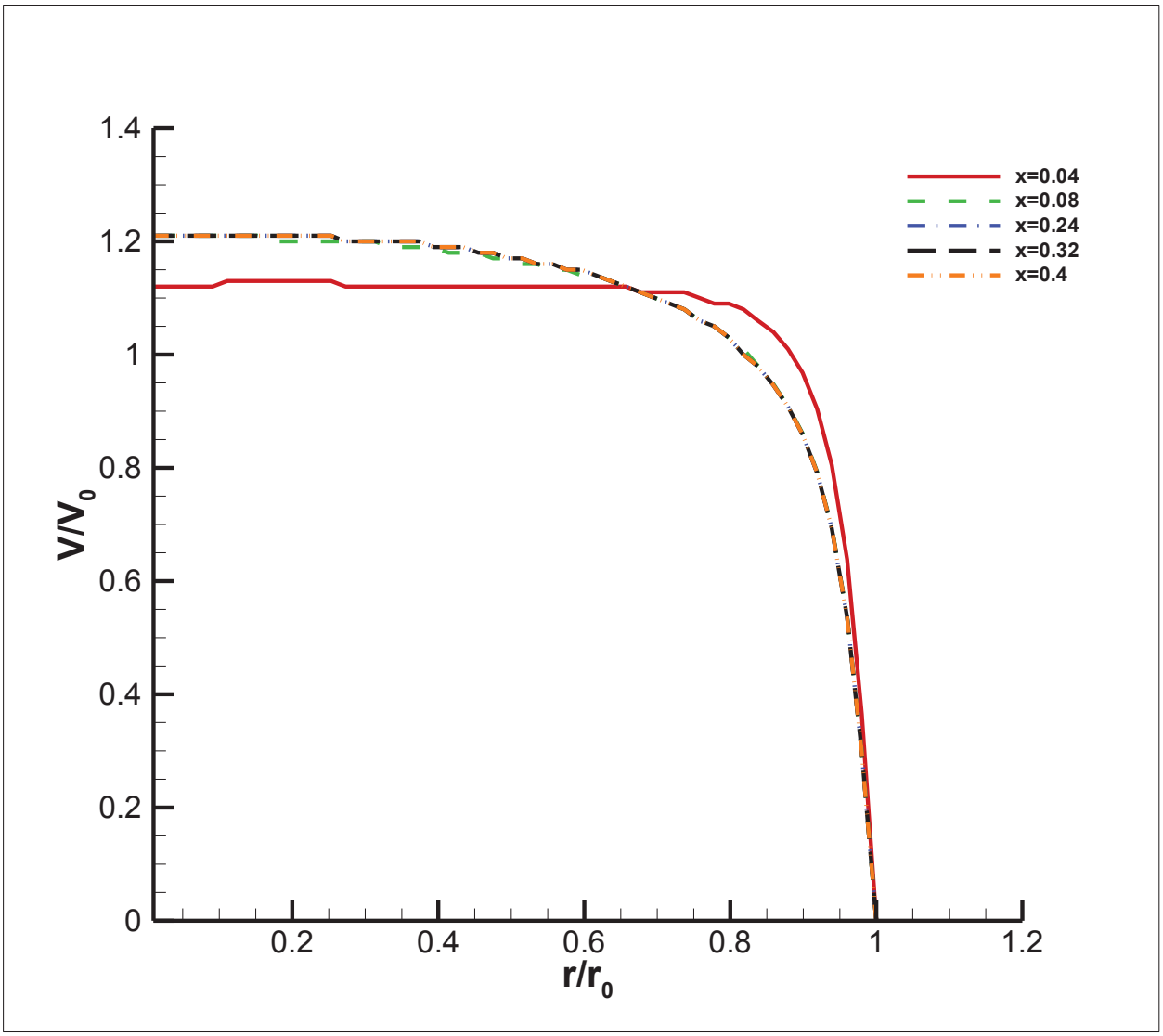

Figure 7. Radial velocity profiles for q = 2089.56 W/m^2 and Re = 6020 and = 3%.

flow, as expected. This is because when the fluid just enters the pipe, the boundary layer thickness gradually increases from zero moving in the direction of fluid flow, it eventually reaches the pipe center and fills the pipe, and this happens faster in turbulent flow than in laminar flow hence a shorter entry length. Also, the dependence of the entry length on Reynolds number in the turbulent flow case is weaker compared to laminar flow as can be seen from the relationship that Reynolds number is to the one-fourth power in the turbulent flow case.

When the single-phase model is considered for constant properties, the velocity profiles and hydrodynamics entrance length for ϕ = 0% and ϕ = 3% and *Re* = 1420 lie on each other. This shows that nanoparticles move with the fluid velocity and the velocity profile and hydrodynamic entrance length are independent on nanoparticles concentration values. The velocity axial profiles at x/L for ϕ = 0% and 3% are shown in Fig. 8.

In turbulent flow case, *Re* = 6020 it was observed that in contrast to laminar flow the nanoparticles have a different velocity from the fluid velocity and the velocity profile and hydrodynamic entrance length are dependent on nanoparticles concentration values since the plots overlap as can be seen in Fig. 9.

Fig 10 (a) and (b) shows the comparison of the dimensionless temperature profiles for ϕ = 0% and ϕ = 3% respectively at various locations along the tube for *Re* = 1420. A reduction of 2.9 % in the dimensionless temperature profile at *x* = 1.8 m with respect to the base fluid and the wall. Additionally, it can be seen that since the increase of volume fraction increases viscosity and Prandtl number, a longer thermal entrance length results.

Fig 11 (a) and (b) shows the comparison of the dimensionless temperature profiles for ϕ = 0% and ϕ = 3% respectively at several locations along the tube for *Re* = 6020. It can be observed that the shape is changing and it follows the logarithmic thermal profile for turbulent flow for both cases.

To show which of the multiphase models used to model nanofluid predict the heat transfer coefficient more accurately, experimental data of Kim et al. [31] for laminar flow of *Re* = 1460 and ϕ = 3% for Al_2O_3/water nanofluid flow inside a circular tube subjected to a constant wall heat flux was plotted along with the local heat transfer coefficients predicted by the models in Fig. 12 and Fig. 13.

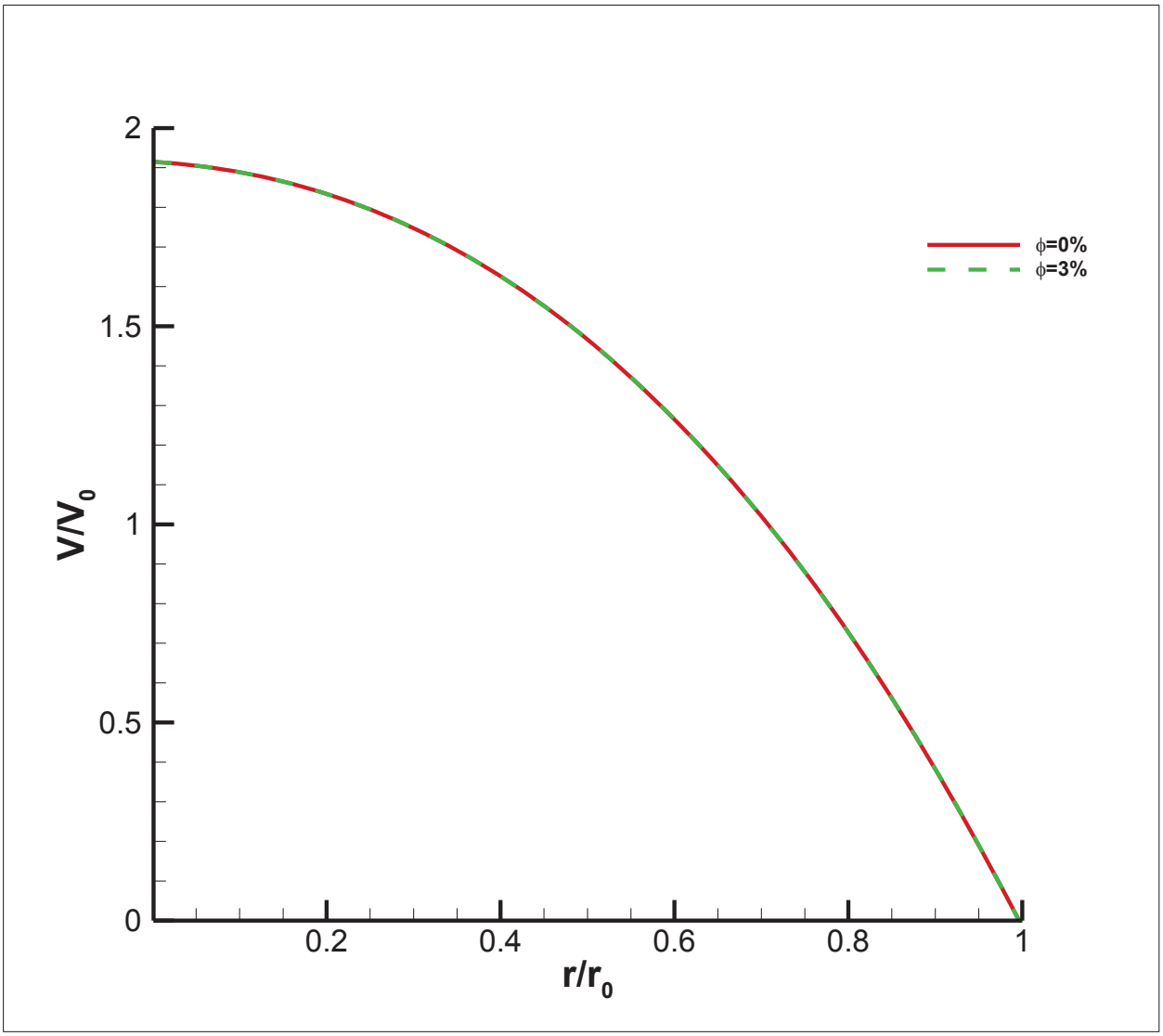

Figure 8. Radial velocity profile for q = 2089.56W/m^2, Re = 1420 at x/L = 0.4 for = 0% and = 3%.

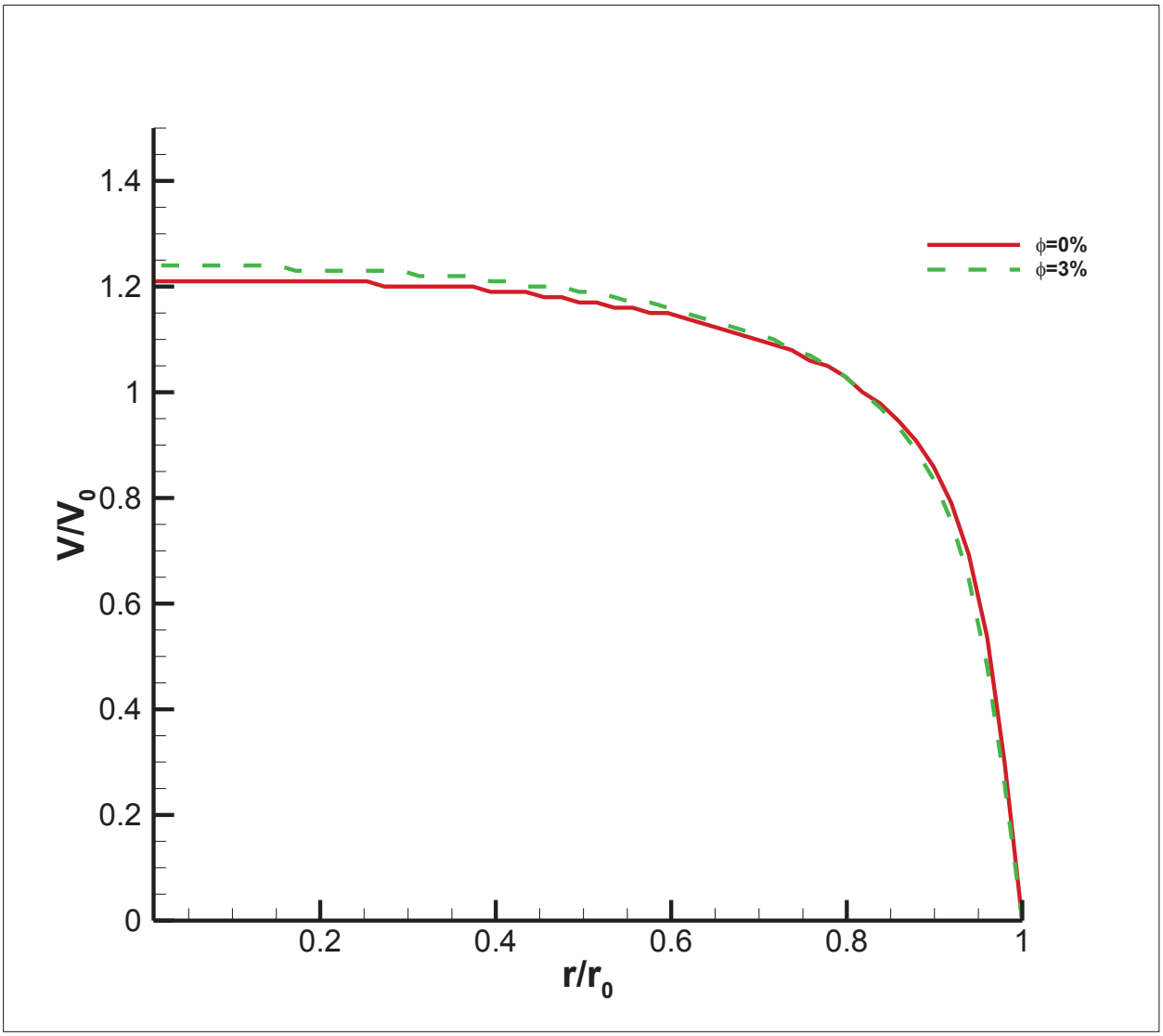

Figure 9. Radial velocity profile for q = 2089.56 W/m^2, Re = 6020 at x/L = 0.4 for = 0% and = 3%.

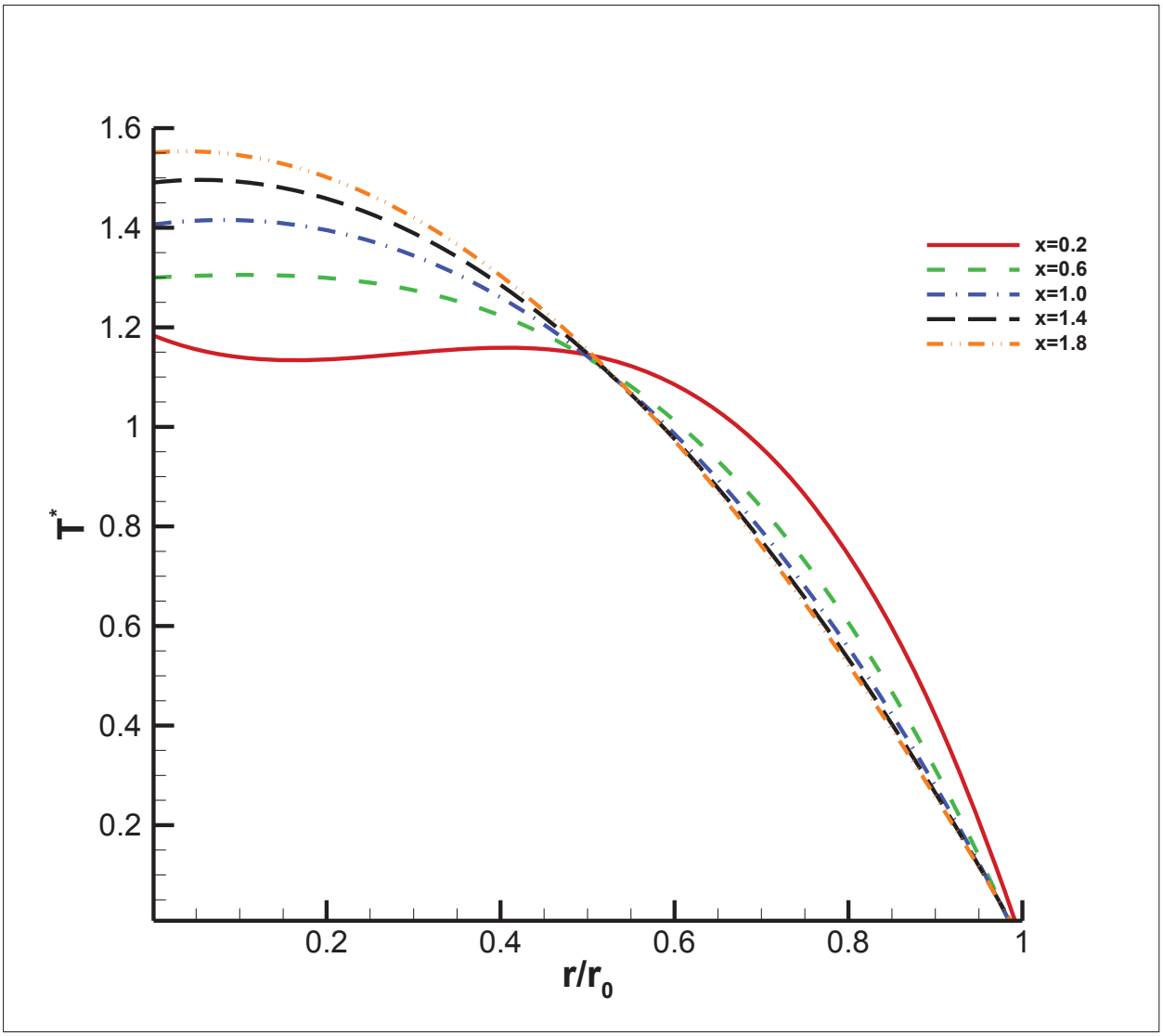

Figure 10(a)

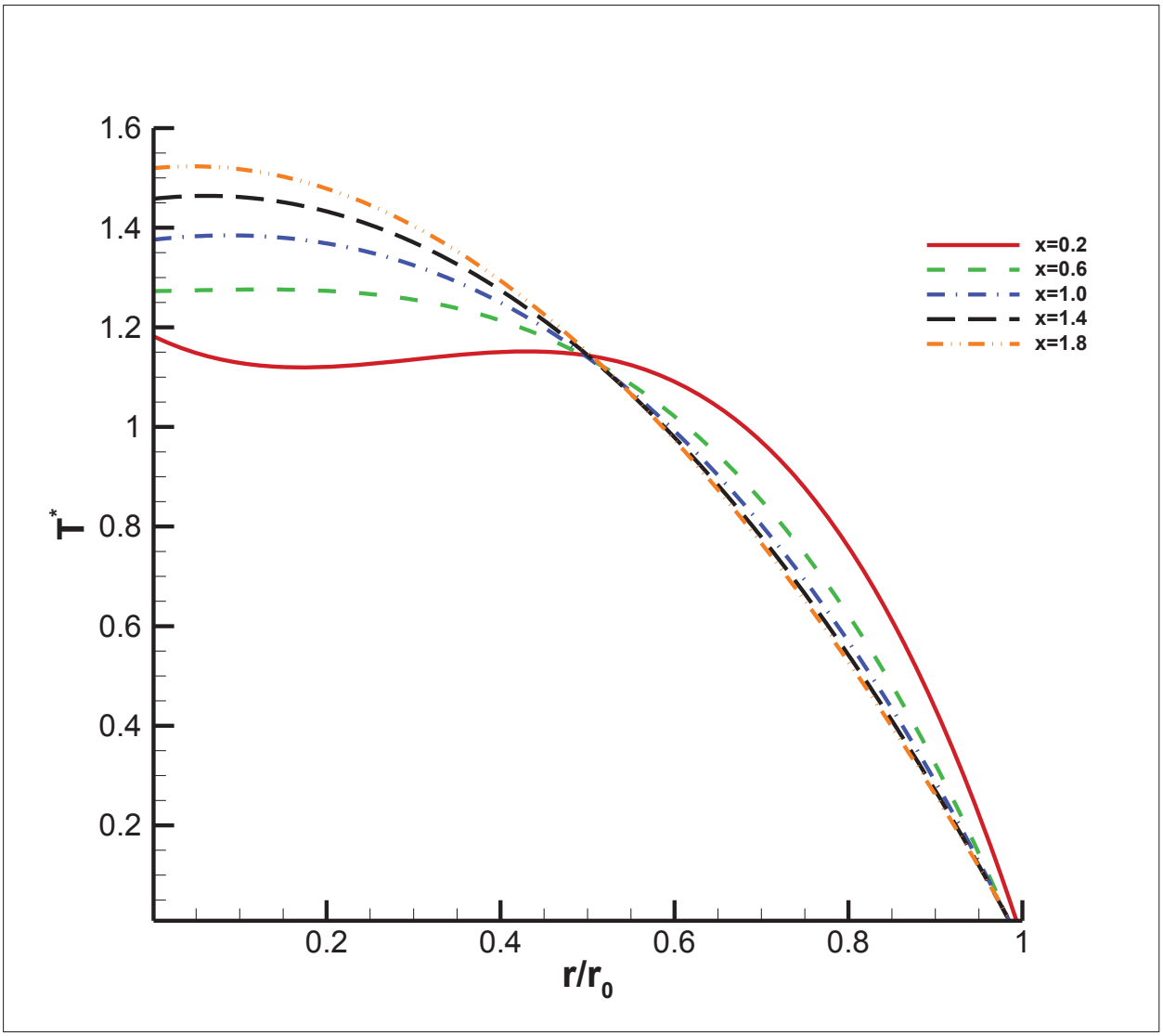

Figure 10(b)

Figure 10. Dimensionless temperature for $q = 2089.56$ W/m^2 and $Re = 1420$ at different axial locations for: (a) = 0% (b) = 3%

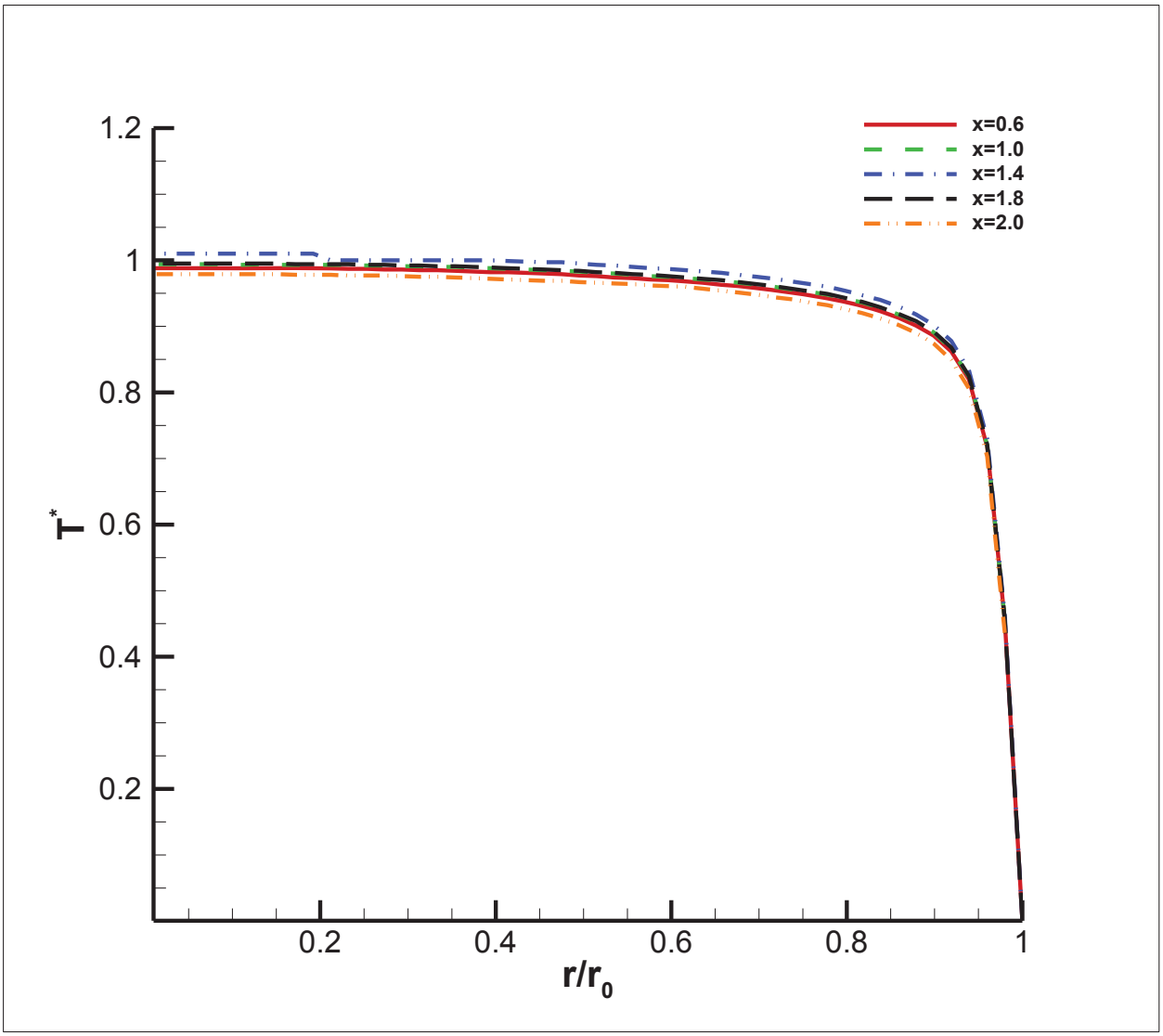

Figure 11(a)

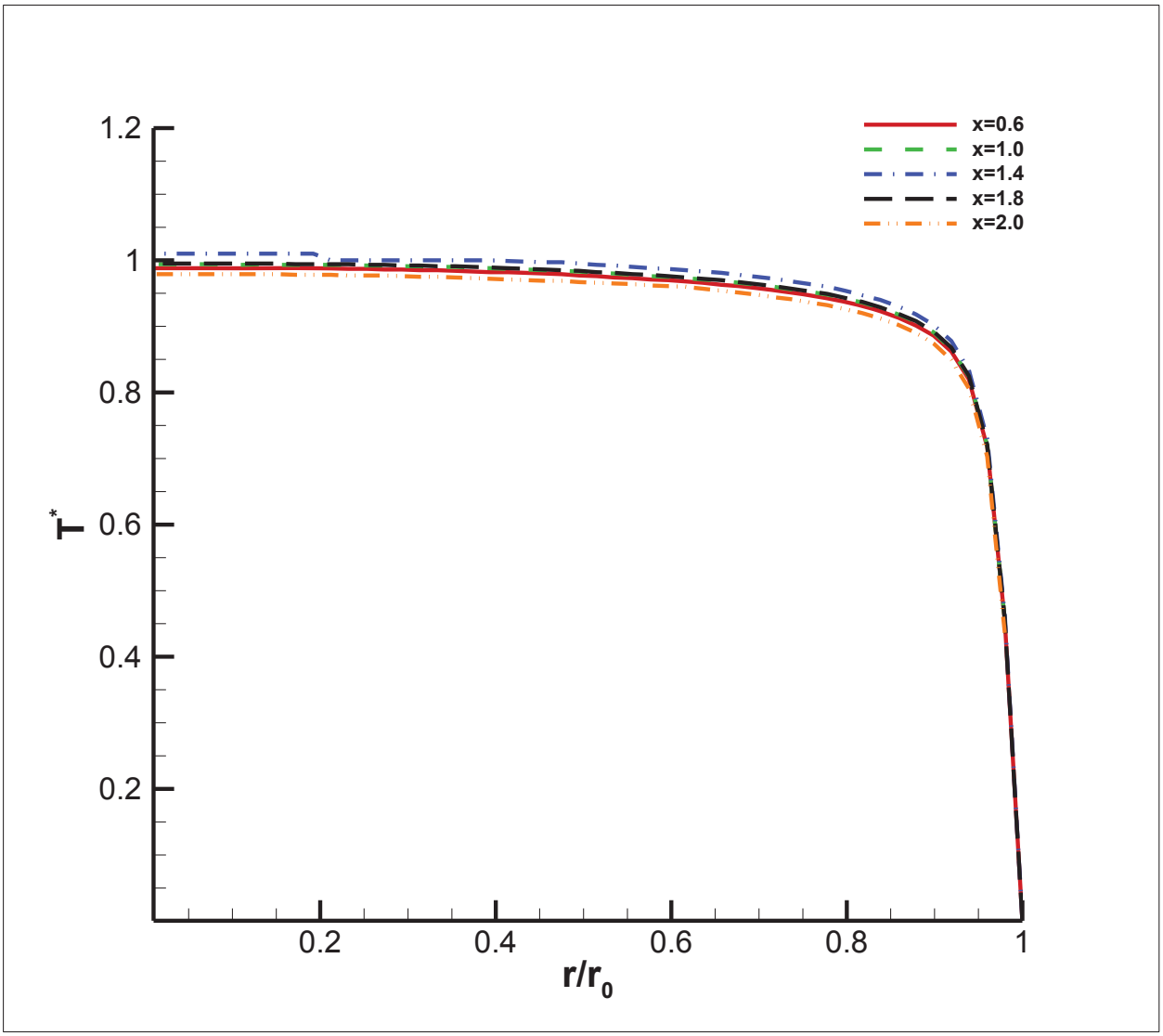

Figure 11(b)

Figure 11. Dimensionless temperature for q = 2089.56 W/m^2 and Re = 6020 at different axial locations for: (a) = 0% (b) = 3%

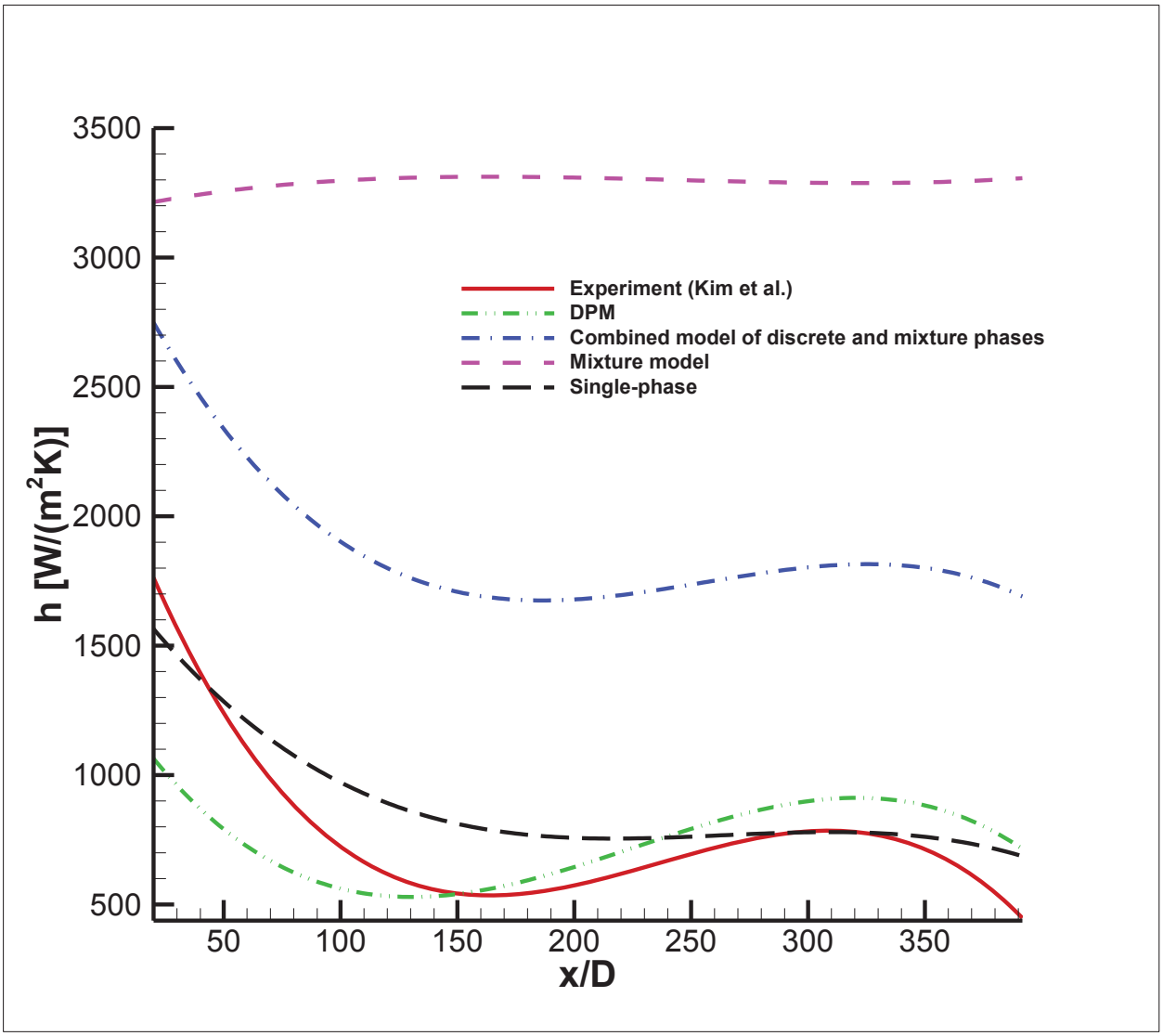

Figure 12. Comparison of the multiphase models with constant properties assumption with experimental data of Kim et al. [31] with = 1420.

Fig. 12 was for constant properties assumption. It can be seen that the mixture model and the combined model of discrete and mixture phases overpredicts the local heat transfer coefficient while the single-phase model deviates from the experimental data at the midsection, the discrete phase model underestimates it at the entrance but gives good predictions elsewhere. It should be noted that constant property assumption is an approximation of the real conditions since transport properties of most fluids vary with temperature hence it was not expected to give results that are more accurate than variable property assumption.

From Fig. 13 for temperature dependent or sometimes called variable properties, it can be seen that the mixture model and the combined model of discrete and mixture phases overpredicts the local heat transfer coefficient while both the discrete phase and single phase models give good predictions and closely follows the experimental data. The average deviation of the discrete phase model from experimental data of Kim et al. [31] was 9%, and the average deviation of the DPM from single phase model was 4.25%.

Fig 14. and Fig.15 is used to show which of the multiphase models used to model nanofluids predicted most accurately the local heat transfer coefficients under turbulent flow conditions. For this purpose, the experimental data of Kim et al. [31] for turbulent flow of Re = 6020 and ϕ = 3% for Al_2O_3/water nanofluid flow inside a circular tube subjected to a constant wall heat flux was compared to the local heat transfer coefficients predicted by the models. It can be deduced from Fig. 14 for constant properties assumption, that the mixture and the combined model of discrete and mixture phases gave similar results but overpredicted the local heat transfer coefficients. However, the single-phase model underestimates it. It was also found that the discrete phase model closely predicted the local heat transfer coefficient at the entrance region after which it began to fail, The average deviation was 13% from the experimental data of Kim et al. [31]. In addition, it can be seen from Fig. 14 that the discrete phase model gave better results than the other models studied for constant properties assumption.

It can be observed from Fig. 15 for temperature dependent properties, that the mixture, combined model of discrete and mixture phases overpredicted the local heat transfer coefficient while the discrete phase and single-phase models give similar results which are closer to experimental data by Kim et al. [31]. However, the discrete phase model accurately predicts the local heat transfer coefficient of the nanofluid at the entrance region and has an average deviation of less than 9%

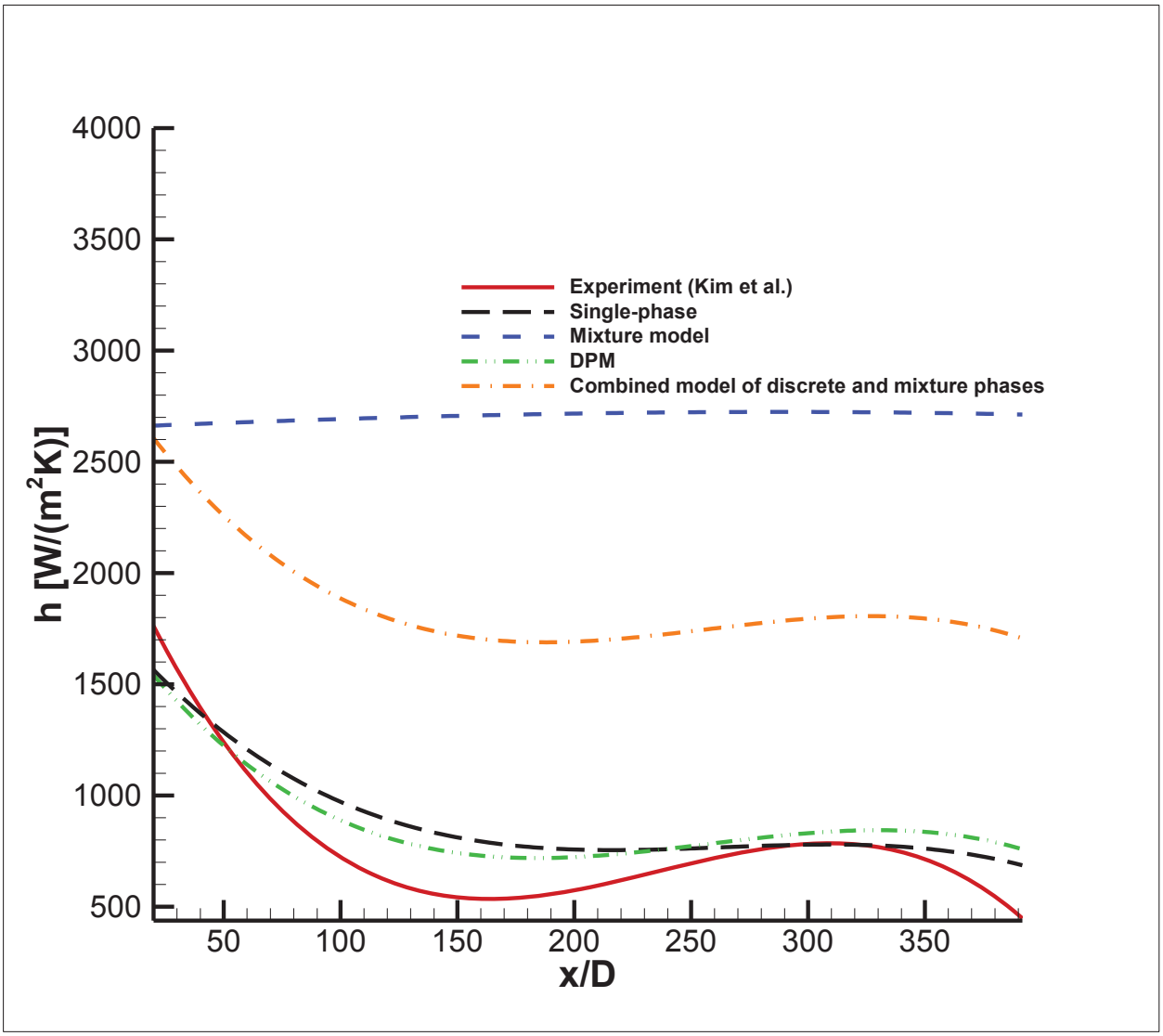

Figure 13. Comparison of the multiphase models with variable property assumption with the experimental data of Kim et al. [31] with = 1420.

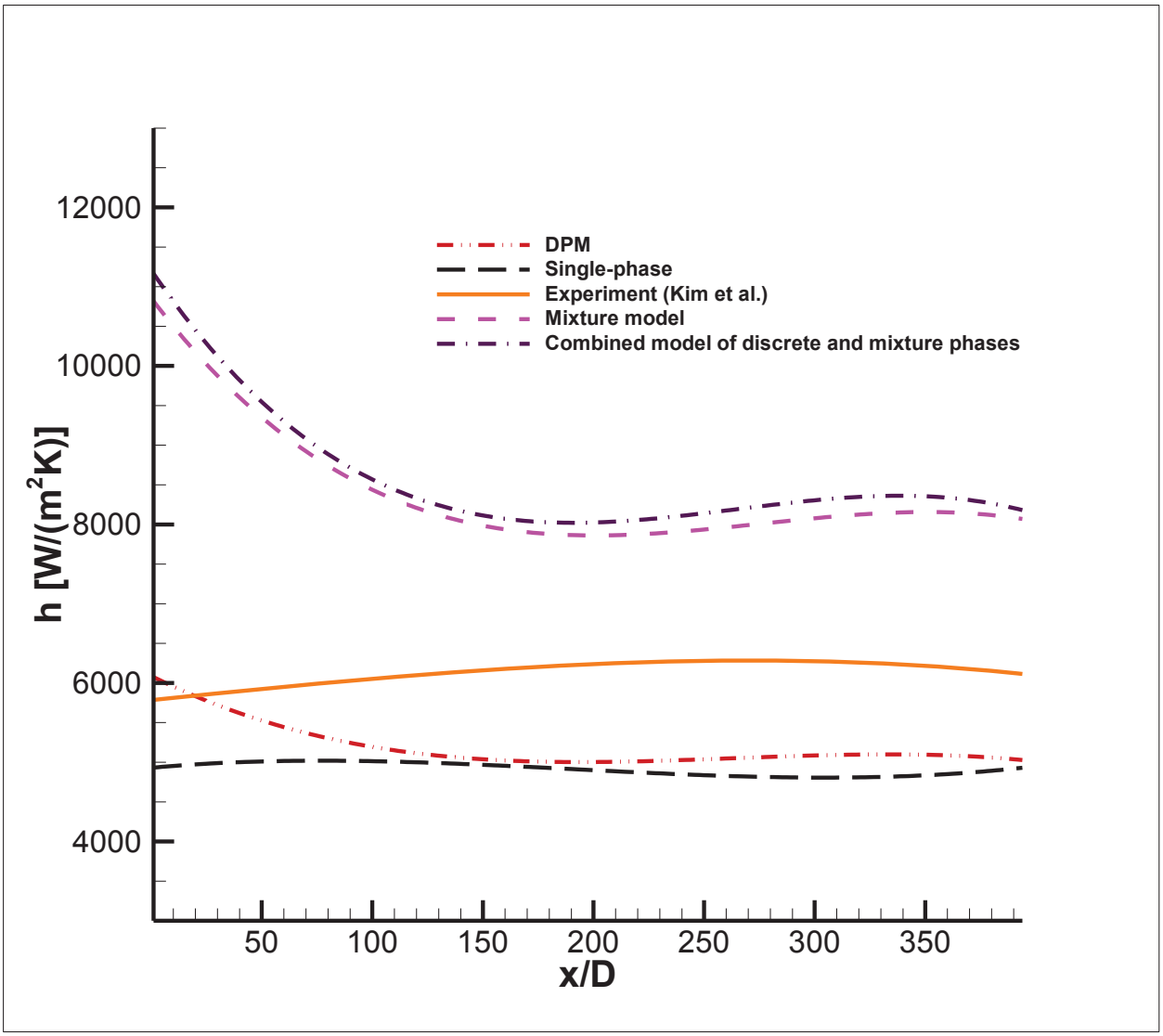

Figure 14. Comparison of the multiphase models with constant property assumption with experimental data of Kim et al. [31] with *Re* = 6020.

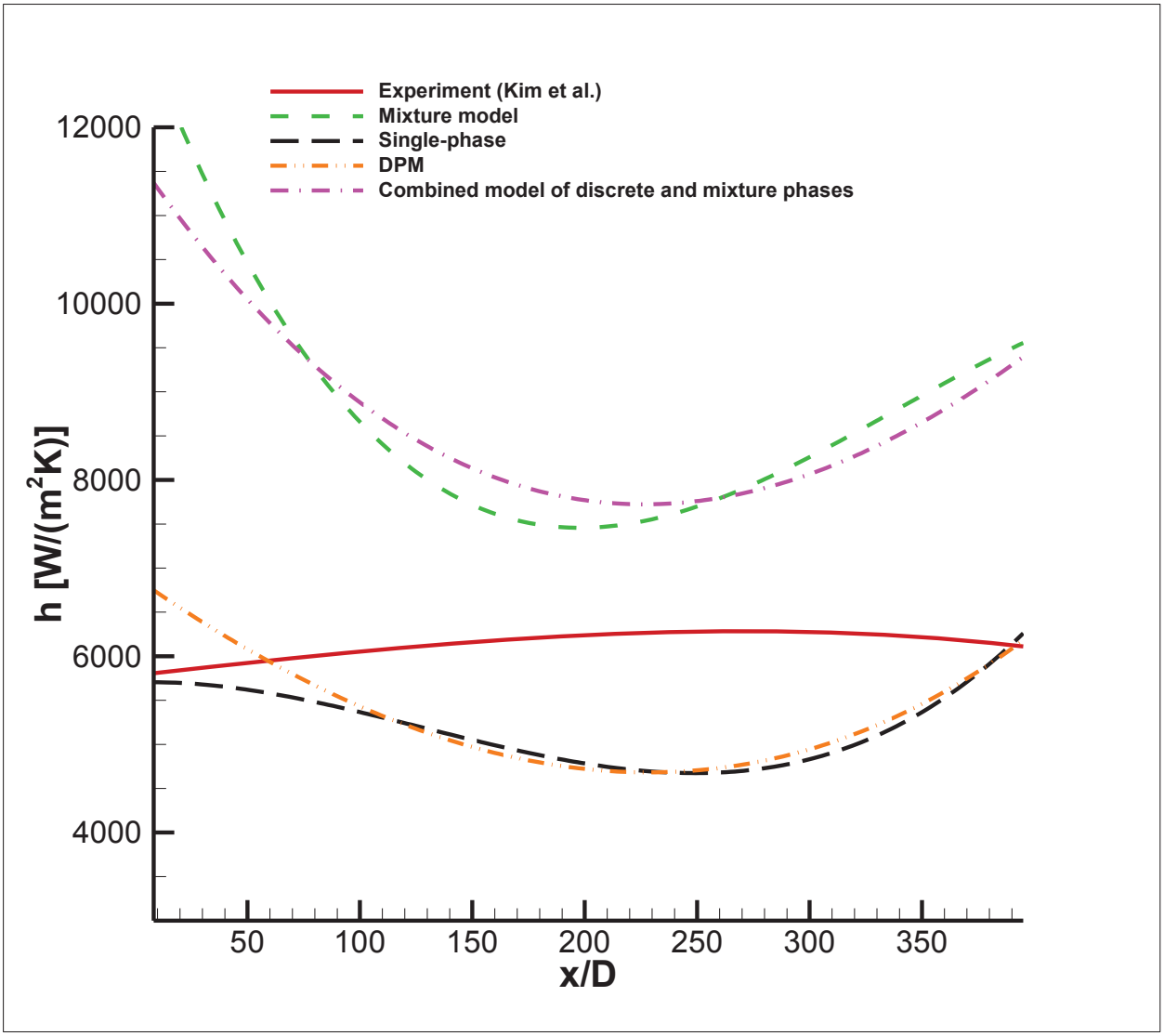

Figure 15. Comparison of the multiphase models with variable property assumption with experimental data of Kim et al. [31] with Re = 6020.

from experimental data of Kim et al. [31]. On the other hand, the average deviation between the single-phase model and the DPM was 2% as the single-phase model underestimated the heat transfer coefficient at the entrance region while the DPM overestimated it at the early entrance region.

From Fig. 16 for laminar flow conditions (Re = 1420), it can be seen that the mixture model and combined model of discrete and mixture phases overpredicts the average Nusselt number for ϕ = 1%, 2%, 3% for both constant and variable properties. While the DPM and single phase models give similar results between the same range of volume fractions. This is because they capture important nanofluid phenomenon which the other models fails to capture. It should be noted that the single phase model only solves based on known correlations hence it can only be as accurate as the correlation at various nanoparticle volume fraction. Additionally the DPM has shown to give good results at many nanoparticle volume fractions; however, there is a limiting volume fraction of 10% above which DPM fails due to a violation of the assumption of no particle-particle interactions.

It can also be observed in Fig. 17 for turbulent flow (Re = 6020), that the mixture model and combined model of discrete and mixture phases give unrealistic results for ϕ = 1%, 2%, 3%, while as with laminar flow the DPM and single phase models give similar results for the same range of volume fractions. Additionally, it can be observed from the plot that SPM cst, SPM var, DPM cst, and the combined model of discrete and mixture phases cst show an optimum range of volume fraction of 1.5 – 2.5% in a bell shaped curve under turbulent flow regime. This is due to the fact that as more particles are added to the base fluid it increases its thermal conductivity and hence heat transfer by conduction increases hence the Nusselt number drops. It should be noted that this trend is not observed in all the models; the reason could be that they may have their own local optimum values.

7. Conclusion

A three-dimensional model considering nanofluid flow for the laminar and turbulent flow was studied. The DPM, single-phase, mixture, combined model of discrete and mixture phases, each with either constant or variable properties were investigated. For the turbulent flow regime, it

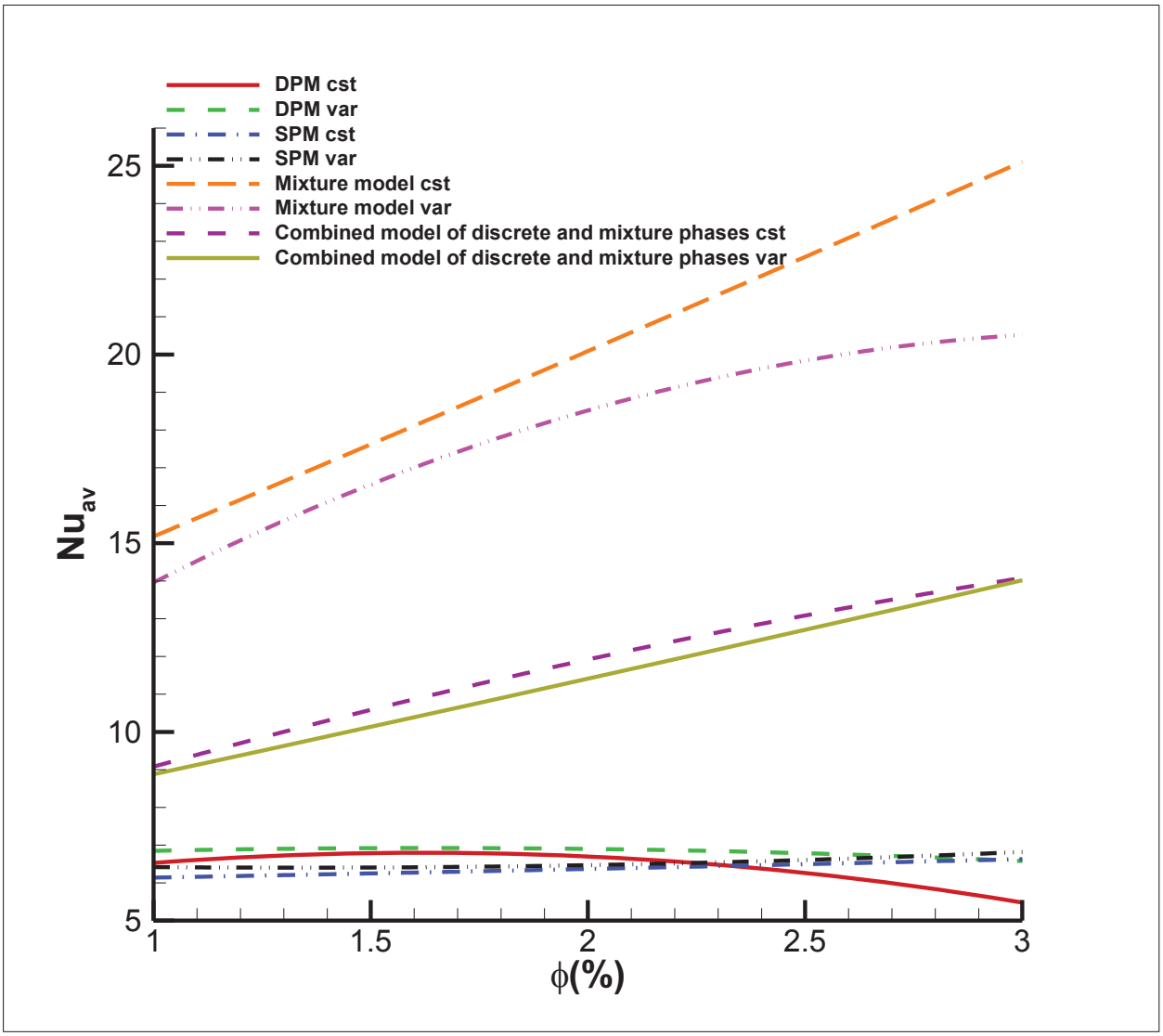

Figure 16. The plot of the average Nusselt number and volume fraction for all models studied under laminar flow.

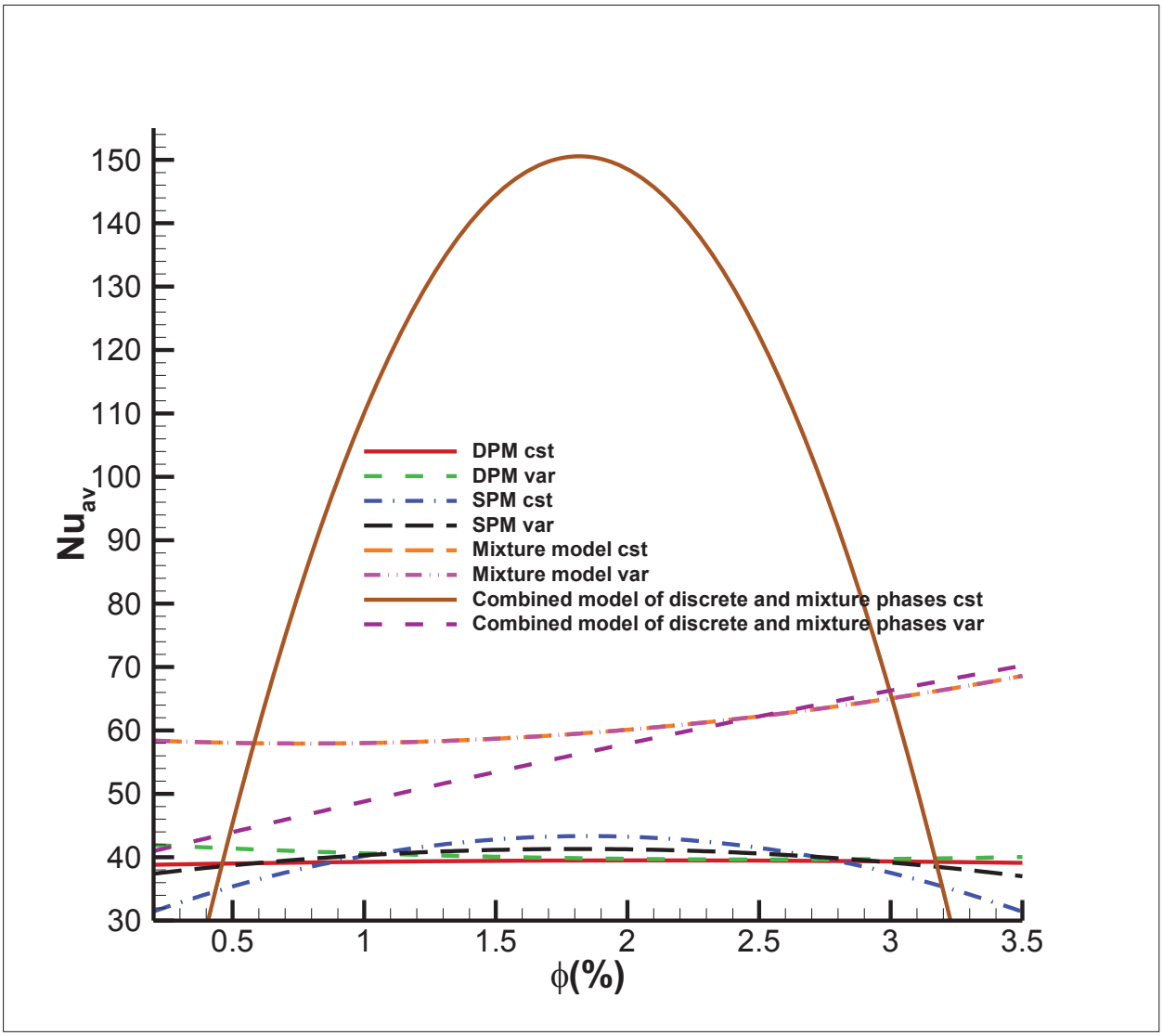

Figure 17. The plot of the average Nusselt number and volume fraction for all models studied under turbulent flow.

was found that the DPM with variable properties predicted the local heat transfer coefficients with an average deviation of less than 9%, the discrete phase model deviated from the single-phase model by less than 2%. For the laminar flow regime, it was found that the discrete phase model with variable properties predicts the local heat transfer coefficient accurately at the exit and entrance region of the pipe and it deviates by 9% and its average deviation from the single phase model was 4.25%, while the single-phase model predicts the local heat transfer coefficient better with constant property assumption. Also, using the single-phase model requires that correlation of thermo-physical properties be ready at hand which significantly limits its use although it is less computationally tasking. From the results presented, the discrete phase model is suggested for the simulation of nanofluid given its accuracy and none dependence on the thermo-physical correlation of the particular nanofluid in the question. However, more studies should be carried out to accommodate particle coalescence in the DPM and include other flow phenomenon of nanofluid.

Conflict of Interest

There is no conflict of interest. This manuscript has not been submitted to anywhere else.

References

[1] S. Mirmasoumi, A. Behzadmehr, Numerical study of laminar mixed convection of a nanofluid in a horizontal tube using two-phase mixture model, Applied Thermal Engineering, 28 (2008) 717-727.
[2] S. Wang, J. Sun, Q. Yang, Y. Zhao, J. Gao, Y. Liu, Numerical simulation of flow behavior of particles in an inverse liquid–solid fluidized bed, Powder Technology, 261 (2014) 14-21.
[3] S. Wang, X. Jiang, R. Wang, X. Wang, S. Yang, J. Zhao, Y. Liu, Numerical simulation of flow behavior of particles in a liquid-solid stirred vessel with baffles, Advanced Powder Technology, 28 (2017) 1611-1624.
[4] M. Marzougui, M. Hammami, R.B. Maad, Numerical simulation into the convective heat transfer of Al_2O_3 and CuO nanofluids flowing through a straight tube using the two phase modeling, Nanoscience and Nanotechnology, 6 (2016) 122-131.
[5] M.N. Labib, M.J. Nine, H. Afrianto, H. Chung, H. Jeong, Numerical investigation on effect of base fluids and hybrid nanofluid in forced convective heat transfer, International Journal of Thermal Sciences, 71 (2013) 163-171.

[6] V. Bianco, F. Chiacchio, O. Manca, S. Nardini, Numerical investigation of nanofluids forced convection in circular tubes, Applied Thermal Engineering, 29 (2009) 3632-3642.
[7] B. Kristiawan, B. Santoso, W.E. Juwana, R.M. Ramadhan, I. Riandana, Numerical investigation of laminar convective heat transfer for TiO_2/water nanofluids using two-phase mixture model (Eulerian approach), in: AIP Conference Proceedings, AIP Publishing, 2017.
[8] Y. He, Y. Men, Y. Zhao, H. Lu, Y. Ding, Numerical investigation into the convective heat transfer of TiO_2 nanofluids flowing through a straight tube under the laminar flow conditions, Applied Thermal Engineering, 29 (2009) 1965-1972.
[9] S. Özerinç, A. Yazıcıoğlu, S. Kakaç, Numerical analysis of laminar forced convection with temperature-dependent thermal conductivity of nanofluids and thermal dispersion, International Journal of Thermal Sciences, 62 (2012) 138-148.
[10] F. Garoosi, F. Talebi, Numerical analysis of conjugate natural and mixed convection heat transfer of nanofluids in a square cavity using the two-phase method, Advanced Powder Technology, 28 (2017) 1668-1695.
[11] V. Bianco, O. Manca, S. Nardini, Numerical investigation on nanofluids turbulent convection heat transfer inside a circular tube, International Journal of Thermal Sciences, 50 (2011) 341-349.
[12] M. Sharifpur, A.B. Solomon, J.P. Meyer, J. S. Ibrahim, E. Barki, Thermal conductivity and viscosity of Mango bark/water nanofluids, in: 13th International Conference on Heat Transfer, Fluid Mechanics and Thermodynamics, 2017, pp. 17-19.
[13] A.B. Solomon, M. Sharifpur, J. P. Meyer, J. S. Ibrahim, E. Barki, Convection heat transfer with water based mango bark nanofluids, (2017).
[14] S.U. Choi, J.A. Eastman, Enhancing thermal conductivity of fluids with nanoparticles, in, Argonne National Lab., IL (United States), 1995.
[15] S. Kakaç, A. Pramuanjaroenkij, Review of convective heat transfer enhancement with nanofluids, International Journal of Heat and Mass Transfer, 52 (2009) 3187-3196.
[16] H. Hadi Najafabadi, M. Keshavarz Moraveji, CFD investigation of local properties of Al_2O_3/water nanofluid in a converging microchannel under imposed pressure difference, Advanced Powder Technology, 28 (2017) 763-774.
[17] M. Shafahi, V. Bianco, K. Vafai, O. Manca, Thermal performance of flat-shaped heat pipes using nanofluids, International Journal of Heat and Mass Transfer, 53 (2010) 1438-1445.
[18] K. Alizad, K. Vafai, M. Shafahi, Thermal performance and operational attributes of the startup characteristics of flat-shaped heat pipes using nanofluids, International Journal of Heat and Mass Transfer, 55 (2012) 140-155.
[19] P. Vassallo, R. Kumar, S.D. Amico, Pool boiling heat transfer experiments in silica–water nanofluids, International Journal of Heat and Mass Transfer, 47 (2004) 406-411.
[20] K. Khanafer, K. Vafai, M. Lightstone, Buoyancy-driven heat transfer enhancement in a two-dimensional enclosure utilizing nanofluids, International Journal of Heat and Mass Transfer, 46 (2003) 3639-3653.
[21] M. Ghanbarpour, R. Khodabandeh, K. Vafai, An investigation of thermal performance improvement of a cylindrical heat pipe using Al_2O_3 nanofluid, Heat and Mass Transfer, 53 (2017) 973-983.
[22] K. Khanafer, K. Vafai, A critical synthesis of thermophysical characteristics of nanofluids, International Journal of Heat and Mass Transfer, 54 (2011) 4410-4428.

[23] K. Milani Shirvan, M. Mamourian, R. Ellahi, Numerical investigation and optimization of mixed convection in ventilated square cavity filled with nanofluid of different inlet and outlet port, International Journal of Numerical Methods for Heat & Fluid Flow, 27 (2017) 2053-2069.
[24] N. Ijaz, A. Zeeshan, M. Bhatti, R. Ellahi, Analytical study on liquid-solid particles interaction in the presence of heat and mass transfer through a wavy channel, Journal of Molecular Liquids, 250 (2018) 80-87.
[25] M. Bahiraei, R. Khosravi, S. Heshmatian, Assessment and optimization of hydrothermal characteristics for a non-Newtonian nanofluid flow within miniaturized concentric-tube heat exchanger considering designer's viewpoint, Applied Thermal Engineering, 123 (2017) 266-276.
[26] M. Bahiraei, K. Gharagozloo, M. Alighardashi, N. Mazaheri, CFD simulation of irreversibilities for laminar flow of a power-law nanofluid within a minichannel with chaotic perturbations: An innovative energy-efficient approach, Energy Conversion and Management, 144 (2017) 374-387.
[27] R. Ellahi, A. Zeeshan, N. Shehzad, S.Z. Alamri, Structural impact of kerosene-Al_2O_3 nanoliquid on MHD Poiseuille flow with variable thermal conductivity: Application of cooling process, Journal of Molecular Liquids, 264 (2018) 607-615.
[28] M. Bhatti, A. Zeeshan, R. Ellahi, G. Shit, Mathematical modeling of heat and mass transfer effects on MHD peristaltic propulsion of two-phase flow through a Darcy-Brinkman-Forchheimer porous medium, Advanced Powder Technology, 29 (2018) 1189-1197.
[29] S. Rashidi, S. Akar, M. Bovand, R. Ellahi, Volume of fluid model to simulate the nanofluid flow and entropy generation in a single slope solar still, Renewable Energy, 115 (2018) 400-410.
[30] R. Ellahi, Special issue on recent developments of nanofluids, in, Multidisciplinary Digital Publishing Institute, 2018.
[31] D. Kim, Y. Kwon, Y. Cho, C. Li, S. Cheong, Y. Hwang, J. Lee, D. Hong, S. Moon, Convective heat transfer characteristics of nanofluids under laminar and turbulent flow conditions, Current Applied Physics, 9 (2009) 119-123.
[32] R. Lotfi, Y. Saboohi, A. Rashidi, Numerical study of forced convective heat transfer of nanofluids: comparison of different approaches, International Communications in Heat and Mass Transfer, 37 (2010) 74-78.
[33] M. Mahdavi, Study of flow and heat transfer features of nanofluids using multiphase models: Eulerian multiphase and discrete Lagrangian approaches, in, University of Pretoria, 2017.
[34] S.E.B. Maiga, S.J. Palm, C.T. Nguyen, G. Roy, N. Galanis, Heat transfer enhancement by using nanofluids in forced convection flows, International Journal of Heat and Fluid flow, 26 (2005) 530-546.
[35] A. Albojamal, K. Vafai, Analysis of single phase, discrete and mixture models, in predicting nanofluid transport, International Journal of Heat and Mass Transfer, 114 (2017) 225-237.
[36] M. Mahdavi, M. Sharifpur, J.P. Meyer, CFD modelling of heat transfer and pressure drops for nanofluids through vertical tubes in laminar flow by Lagrangian and Eulerian approaches, International Journal of Heat and Mass Transfer, 88 (2015) 803-813.
[37] M. Mahdavi, M. Sharifpur, J.P. Meyer, Simulation study of convective and hydrodynamic turbulent nanofluids by turbulence models, International Journal of Thermal Sciences, 110 (2016) 36-51.
[38] M. Bahiraei, M. Jamshidmofid, S. Heshmatian, Entropy generation in a heat exchanger working with a biological nanofluid considering heterogeneous particle distribution, Advanced Powder Technology, 28 (2017) 2380-2392.

[39] M. Sheikholeslami, H.B. Rokni, Free convection of $CuO–H_2O$ nanofluid in a curved porous enclosure using mesoscopic approach, International Journal of Hydrogen Energy, 42 (2017) 14942-14949.
[40] M.K. Moraveji, R.M. Ardehali, CFD modeling (comparing single and two-phase approaches) on thermal performance of Al2O3/water nanofluid in mini-channel heat sink, International Communications in Heat and Mass Transfer, 44 (2013) 157-164.
[41] S.A.M. Mehryan, F.M. Kashkooli, M. Ghalambaz, A.J. Chamkha, Free convection of hybrid Al_2O_3-Cu water nanofluid in a differentially heated porous cavity, Advanced Powder Technology, 28 (2017) 2295-2305.
[42] I. Behroyan, S.M. Vanaki, P. Ganesan, R. Saidur, A comprehensive comparison of various CFD models for convective heat transfer of Al_2O_3 nanofluid inside a heated tube, International Communications in Heat and Mass Transfer, 70 (2016) 27-37.
[43] M.K. Moraveji, E. Esmaeili, Comparison between single-phase and two-phases CFD modeling of laminar forced convection flow of nanofluids in a circular tube under constant heat flux, International Communications in Heat and Mass Transfer, 39 (2012) 1297-1302.
[44] H. Safikhani, E. Hajian, R. Mohammadi, Numerical simulation of nanofluid flow over diamond-shaped elements in tandem in laminar and turbulent flow, Transport Phenomenon Nano Micro Scales, 5 (2017) 102-110.
[45] M. Bahiraei, S.M. Majd, Prediction of entropy generation for nanofluid flow through a triangular minichannel using neural network, Advanced Powder Technology, 27 (2016) 673-683.
[46] M. Corcione, Empirical correlating equations for predicting the effective thermal conductivity and dynamic viscosity of nanofluids, Energy Conversion and Management, 52 (2011) 789-793.
[47] M. Mehrali, E. Sadeghinezhad, M.A. Rosen, A.R. Akhiani, S. Tahan Latibari, M. Mehrali, H.S.C. Metselaar, Experimental investigation of thermophysical properties, entropy generation and convective heat transfer for a nitrogen-doped graphene nanofluid in a laminar flow regime, Advanced Powder Technology, 27 (2016) 717-727.
[48] M.H. Saidi, H. Tamim, Heat transfer and pressure drop characteristics of nanofluid in unsteady squeezing flow between rotating porous disks considering the effects of thermophoresis and Brownian motion, Advanced Powder Technology, 27 (2016) 564-574.
[49] C.C. Tang, S. Tiwari, M.W. Cox, Viscosity and Friction Factor of Aluminum Oxide–Water Nanofluid Flow in Circular Tubes,, Journal of Nanotechnology in Engineering and Medicine, 4 (2013) 1-6.
[50] R.M. Moghari, A. Akbarinia, M. Shariat, F. Talebi, R. Laur, Two phase mixed convection Al 2 O 3–water nanofluid flow in an annulus, International Journal of Multiphase Flow, 37 (2011) 585-595.
[51] R. Mokhtari Moghari, A. Akbarinia, M. Shariat, F. Talebi, R. Laur, Two phase mixed convection Al2O3–water nanofluid flow in an annulus, International Journal of Multiphase Flow, 37 (2011) 585-595.
[52] M. Manninen, V. Taivassalo, S. Kallio, On the mixture model for multiphase flow,, Technical Research Centre of Finland, 288 (1996) 9-18.

[53] Y. He, Y. Mena, Y. Zhao, H. Lu, Y. Ding, Numerical investigation into the convective heat transfer of TiO2 nanofluids flowing through a straight tube under the laminar flow conditions, Applied Thermal Engineering, 29 (2009) 1965-1972.
[54] T.-H. Shih, W.W. Liou, A. Shabbir, Z. Yang, J. Zhu, A new k-ϵ eddy viscosity model for high reynolds number turbulent flows, Computers & Fluids, 24 (1995) 227-238.

[55] V. Gnielinski, New equations for heat and mass transfer in turbulent pipe and channel flow, International Chemical Engineering, 16 (1976) 359-368.
[56] M. Mahdavi, M. Sharifpur, H. Ghodsinezhad, J.P. Meyer, A new combination of nanoparticles mass diffusion flux and slip mechanism approaches with electrostatic forces in a natural convective cavity flow, International Journal of Heat and Mass Transfer, 106 (2017) 980-988.
[57] P. Keblinski, S.R. Phillpot, S.U.S. Choi, J.A. Eastman, Mechanisms of heat flow in suspensions of nano-sized particles (nanofluids), International Journal of Heat and Mass Transfer, 45 (2002) 855-863.
[58] Q. Li, Y. Xuan, J. Wang, Investigation on convective heat transfer and flow features of nanofluids, Journal of Heat transfer, 125 (2003) 151-155.
[59] G. Saha, Heat transfer perfomance investigation of nanofluids flow in pipe, in: Systems, Power and Energy Division, University of Glasglow, 2016, pp. 232.
[60] M. Mirzaei, M. Saffar-Avval, H. Naderan, Heat transfer investigation of laminar developing flow of nanofluids in a microchannel based on Eulerian–Lagrangian approach, The Canadian Journal of Chemical Engineering, 92 (2014) 1139-1149.
[61] S. El Bécaye Maïga, C. Tam Nguyen, N. Galanis, G. Roy, T. Maré, M. Coqueux, Heat transfer enhancement in turbulent tube flow using Al_2O_3 nanoparticle suspension, International Journal of Numerical Methods for Heat & Fluid Flow, 16 (2006) 275-292.
[62] J.C. Nelson, D. Banerjee, R. Ponnappan, Flow loop experiments using polyalphaolefin nanofluids, Journal of Thermophysics and Heat Transfer, 23 (2009) 752-761.
[63] K.S. Hwang, S.P. Jang, S.U. Choi, Flow and convective heat transfer characteristics of water-based Al_2O_3 nanofluids in fully developed laminar flow regime, International Journal of Heat and Mass transfer, 52 (2009) 193-199.
[64] M. Chandrasekar, S. Suresh, A.C. Bose, Experimental studies on heat transfer and friction factor characteristics of Al_2O_3/water nanofluid in a circular pipe under transition flow with wire coil inserts, Heat Transfer Engineering, 32 (2011) 485-496.
[65] M.S. Mojarrad, A. Keshavarz, M. Ziabasharhagh, M.M. Raznahan, Experimental investigation on heat transfer enhancement of alumina/water and alumina/water–ethylene glycol nanofluids in thermally developing laminar flow, Experimental Thermal and Fluid Science, 53 (2014) 111-118.
[66] E. Esmaeilzadeh, H. Almohammadi, S.N. Vatan, A.N. Omrani, Experimental investigation of hydrodynamics and heat transfer characteristics of Al_2O_3/water under laminar flow inside a horizontal tube, International Journal of Thermal Sciences, 63 (2013) 31-37.
[67] S.Z. Heris, M.N. Esfahany, S.G. Etemad, Experimental investigation of convective heat transfer of Al_2O_3/water nanofluid in circular tube, International Journal of Heat and Fluid Flow, 28 (2007) 203-210.
[68] D. Wen, Y. Ding, Experimental investigation into convective heat transfer of nanofluids at the entrance region under laminar flow conditions, International Journal of Heat and Mass Transfer, 47 (2004) 5181-5188.
[69] K. Sharma, L.S. Sundar, P. Sarma, Estimation of heat transfer coefficient and friction factor in the transition flow with low volume concentration of Al_2O_3 nanofluid flowing in a circular tube and with twisted tape insert, International Communications in Heat and Mass Transfer, 36 (2009) 503-507.
[70] U.U. Rehman, Heat transfer optimization of shell-and-tube heat exchanger through CFD studies, (2012).
[71] N. Rahimpour, M. Keshavarz Moraveji, Free convection of water–Fe_3O_4 nanofluid in an inclined cavity subjected to a magnetic field: CFD modeling, sensitivity analysis, Advanced Powder Technology, 28 (2017) 1573-1584.

[72] R. Davarnejad, S. Barati, M. Kooshki, CFD simulation of the effect of particle size on the nanofluids convective heat transfer in the developed region in a circular tube, SpringerPlus, 2 (2013) 192.
[73] V. Yakhot, S. Orszag, S. Thangam, T. Gatski, C. Speziale, Development of turbulence models for shear flows by a double expansion technique, Physics of Fluids A: Fluid Dynamics, 4 (1992) 1510-1520.
[74] M. Mahdavi, M. Sharifpur, J.P. Meyer, Implementation of diffusion and electrostatic forces to produce a new slip velocity in the multiphase approach to nanofluids, Powder Technology, 307 (2017) 153-162.
[75] M. Mahdavi, M. Sharifpur, J.P. Meyer, A novel combined model of discrete and mixture phases for nanoparticles in convective turbulent flow, Physics of Fluids, 29 (2017) 082005.
[76] M. Mahdavi, M. Sharifpur, J. P. Meyer, Comparative study on simulation of convective AL2O3-water and ZrO2-water nanofluid by using Ansys-Fluent, in: Proceedings of the 15th International Heat Transfer Conference, Kyoto, paper IHTC15-9196, 2014, pp. 10-15.
[77] M. Saberi, M. Kalbasi, A. Alipourzade, Numerical study of forced convective heat transfer of nanofluids inside a vertical tube, International Journal of Thermal Technologies, 3 (2013) 10-15.
[78] M. Hejazian, M.K. Moraveji, A. Beheshti, Comparative numerical investigation on TiO2/water nanofluid turbulent flow by implementation of single phase and two phase approaches, Numerical Heat Transfer, Part A: Applications, 66 (2014) 330-348.
[79] Energy, Why nanoparticles are better than micro-particles, in, Argonne National Laboratory, in, 2004.
[80] S.M. Vanaki, P. Ganesan, H. Mohammed, Numerical study of convective heat transfer of nanofluids: a review, Renewable and Sustainable Energy Reviews, 54 (2016) 1212-1239.
[81] V. Bianco, O. Manca, S. Nardini, K. Vafai, Heat transfer enhancement with nanofluids, CRC press, 2015.
[82] B.C. Pak, Y.I. Cho, Hydrodynamic and heat transfer study of dispersed fluids with submicron metallic oxide particles, Experimental Heat Transfer, 11 (1998) 151-170.
[83] G.F.C. Rogers, Y.R. Mayhew, Thermodynamic and transport properties of fluids, Blackwell Oxford, 1981.
[84] G. McNab, A. Meisen, Thermophoresis in liquids, Journal of Colloid and Interface Science, 44 (1973) 339-346.
[85] ANSYS Academic Research release 18.0 Help system 24.6.12 Coupled Calculations; ANSYS, INC., 2016.
[86] L. Godson, B. Raja, D.M. Lal, S. Wongwises, Enhancement of heat transfer using nanofluids—an overview, Renewable and Sustainable Energy Reviews, 14 (2010) 629-641.
[87] M.S. Mojarrad, A. Keshavarz, A. Shokouhi, Nanofluids thermal behavior analysis using a new dispersion model along with single-phase, Heat and Mass Transfer, 49 (2013) 1333-1343.
[88] S.K. Das, S.U. Choi, W. Yu, T. Pradeep, Nanofluids: science and technology, John Wiley & Sons, 2007.
[89] H. Ounis, G. Ahmadi, J.B. McLaughlin, Brownian diffusion of submicrometer particles in the viscous sublayer, Journal of Colloid and Interface Science, 143 (1991) 266-277.
[90] ANSYS Academic Research, Release 18.0, 2016.
[91] L. Talbot, R. Cheng, R. Schefer, D. Willis, Thermophoresis of particles in a heated boundary layer, Journal of Fluid Mechanics, 101 (1980) 737-758.
[92] W. Minkowycz, E.M. Sparrow, J.Y. Murthy, J.P. Abraham, Handbook of numerical heat transfer, John Wiley & Sons, Inc., 2009.

[93] A. Naumann, L. Schiller, A drag coefficient correlation, Z. Ver. Deutsch. Ing, 77 (1935).
[94] M. Syamlal, W. Rogers, T. O'Brien, MFIX Documentation: Volume 1, Theory Guide. National Technical Information Service, Springfield, VA, 1993.
[95] C. Lun, S.B. Savage, D. Jeffrey, N. Chepurniy, Kinetic theories for granular flow: inelastic particles in Couette flow and slightly inelastic particles in a general flowfield, Journal of Fluid Mechanics, 140 (1984) 223-256.
[96] S.W. Churchill, H. Ozoe, Correlations for laminar forced convection with uniform heating in flow over a plate and in developing and fully developed flow in a tube, Journal of Heat Transfer, 95 (1973) 78-84.
[97] W. Williams, J. Buongiorno, L.-W. Hu, Experimental investigation of turbulent convective heat transfer and pressure loss of alumina/water and zirconia/water nanoparticle colloids (nanofluids) in horizontal tubes, Journal of Heat Transfer, 130 (2008)
[98] W.M. Kays, M.E. Crawford, B. Weigand, Convective heat and mass transfer, 2005.
[99] R.K. Shah, M. Bhatti, Laminar convective heat transfer in ducts, Handbook of single-phase convective heat transfer, 3 (1987).
[100] M. Bhatti, R. Shah, Turbulent and transitional flow convective heat transfer, Hand Book of Single-phase Convection Heat Transfer, in, John Wiley and Sons, New York, 1987.
[101] W. Zhi-qing, Study on correction coefficients of laminar and turbulent entrance region effect in round pipe, Applied Mathematics and Mechanics, 3 (1982) 433-446.